

# Visualization of Electrochemical Reactions in Battery Materials with X-ray Microscopy and Mapping

Mark Wolf, Brian M. May, and Jordi Cabana\*

*Department of Chemistry, University of Illinois at Chicago, Chicago IL*

E-mail: jcabana@uic.edu

## Abstract

Unlocking the full performance capabilities of battery materials will require a thorough understanding of the underlying electrochemical mechanisms at a variety of length scales. A broad arsenal of X-ray microscopy and mapping techniques is now available to probe these processes down to the nano-scale. The tunable nature of X-ray sources allows for the extraction of chemical states through spectromicroscopy. The addition of phase contrast imaging can retrieve the complex-valued refraction of the material, giving an even more nuanced chemical picture. Tomography and coherent Bragg diffraction imaging provide a reconstructed three-dimensional volume of the specimen, as well as internal strain information from the latter. Many recent insights into battery materials have been achieved through the creative use of these, and similar, methods. Experiments performed while the battery is being actively cycled reveal behavior that differs significantly from what is observed at equilibrium and meta-stable conditions. Planned improvements to X-ray source brightness and coherence will extend these techniques by alleviating the current trade-off in time, chemical and spatial resolution.

# Introduction

Beyond the visible consumer electronics applications, energy storage plays a critical role in areas such as manufacturing, transportation and electricity generation. By some estimates, US industries lose \$80 billion each year due to power interruptions, while annual electric vehicle sales are seeing large and consistent increases.<sup>1</sup> Additionally, if renewables are to become the main source of energy production, we will need storage solutions to deal with their intermittent nature. Even with coal and natural gas, fluctuations in demand require that more expensive “peaker plants” be brought online, which could be alleviated if energy from base-load plants can be stored when demand is low. The cheapest energy storage methods, pumped-hydro and compressed-air, are severely limited by the availability of suitable locations. Currently, batteries hold much promise as portable energy storage systems. Batteries contain two electrodes, sites where oxidation and reduction reactions (redox) take place.<sup>2</sup> The fundamental redox chemistry within batteries is non-trivial and governs the practical aspects that are felt by the consumer, such as capacity, cycle life, and power, among others. Therefore, advances in battery technology that yield cheaper, more reliable and better performing systems will result in large economic, environmental and geopolitical benefits. A key requirement for achieving this goal is a better understanding of the chemistry underlying these materials, in order to operate as close as possible to their theoretical limits.

Measuring chemical properties with spatial resolution provides a view of the underlying mechanisms that is not available by looking at bulk properties. Electrodes generally adopt a hierarchical structure wherein single crystallites of a redox-active material combine to form agglomerate particles, which are then combined with conductive additives and flexible polymeric binders into a thick (ideally, above 100  $\mu\text{m}$ ), porous electrode architecture (figure 1) where different distributions of components and particle sizes are likely to exist throughout the electrode, demonstrated in figure 2. In addition, the thickness of the electrode introduces asymmetries in the transport of ions (from the electrolyte) and electrons (from the current collector, figure 2), which are both required in order for the redox reaction to proceed. As a

result, a hierarchy of inhomogeneities develops during the phase transformation, both within the electrode<sup>3,4</sup> and within individual particles. These inhomogeneities are kinetic in origin, beyond the changes that would be inherent to the phase transformation within a particle, and, thus, prone to vary with the currents to which the battery is subjected. Probing all of these length-scales provides clues for helping meet the high demands placed on current technology.

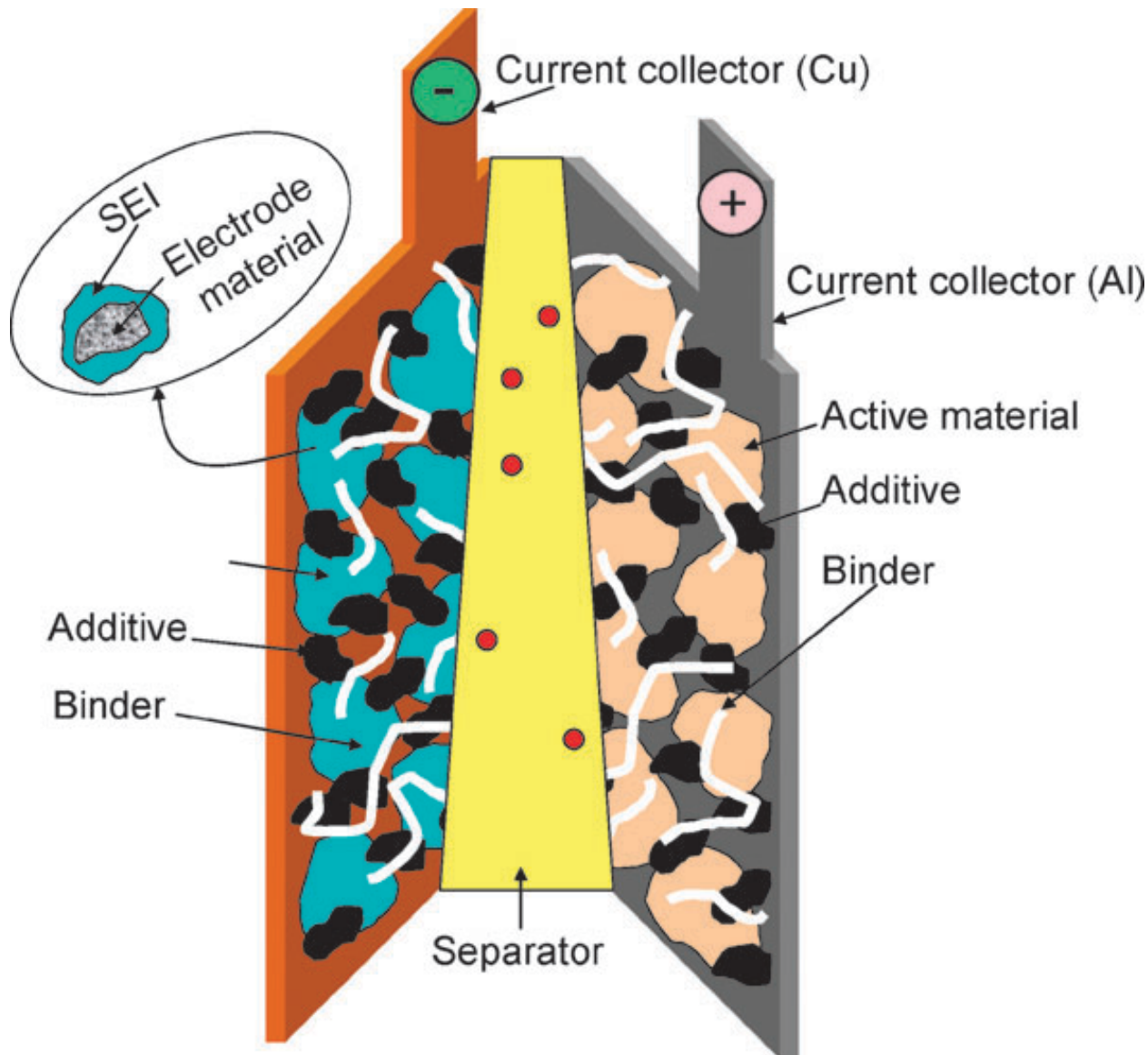


Figure 1: Schematic of a typical battery. The electrodes are made of multiple individual particles that participate in the electrochemical reaction (denoted as “active material”). Reproduced from Ref.<sup>5</sup> with permission from the Royal Society of Chemistry.

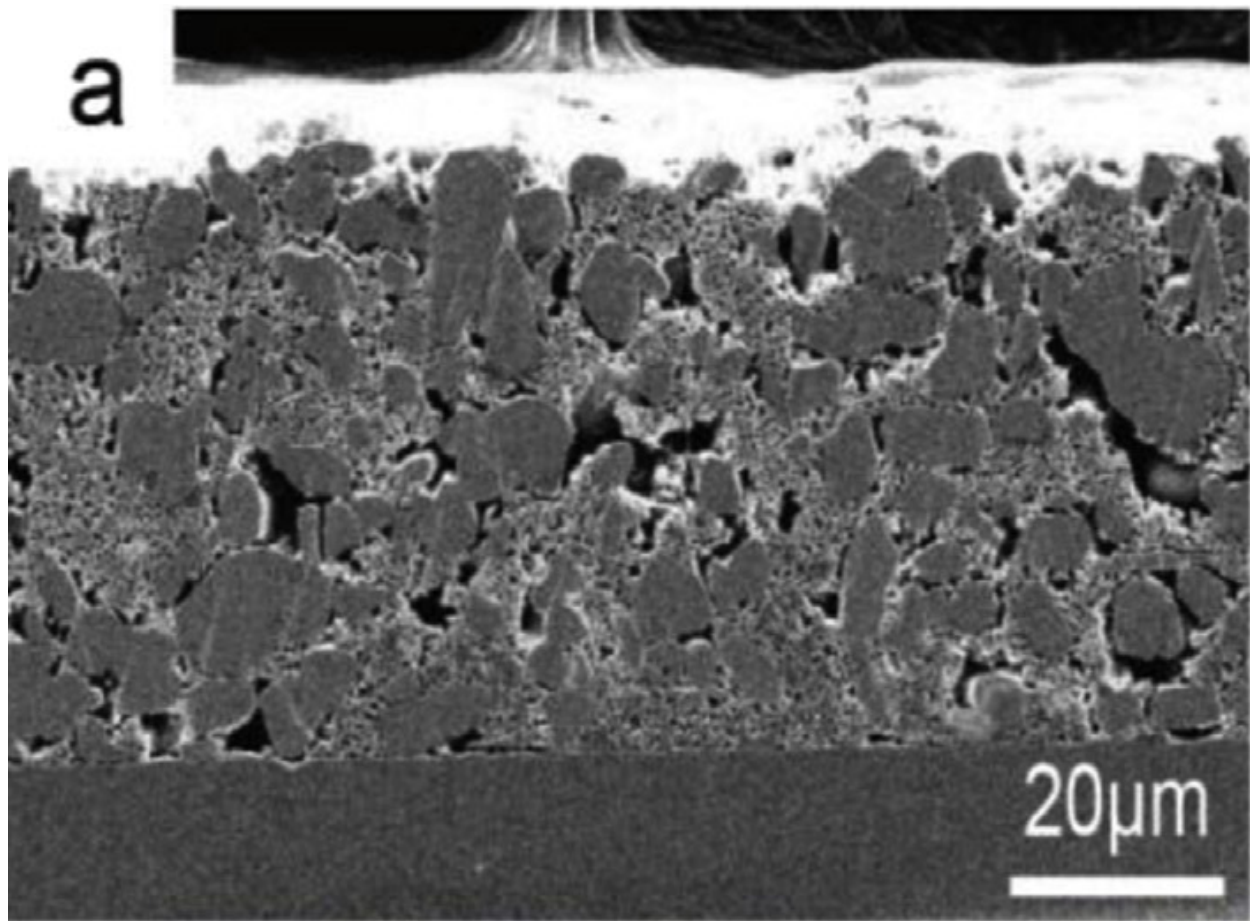


Figure 2: Scanning electron microscope image of the cross-section of a typical battery electrode. Multiple individual particles can be seen that participate in the electrochemical reaction. Reprinted from *Journal of Power Sources*, 252, J. Choi et al., Improved high-temperature performance of lithium-ion batteries through use of a thermally stable co-polyimide-based cathode binder, 138-143, 2014, with permission from Elsevier.

X-rays are able to probe various length scales using a variety of contrast mechanisms. Compared to electron microscopy, another common tool for achieving spatially resolved information from cathode materials, X-rays are significantly less damaging to the material in most conditions. Additionally, transmission electron microscopy (TEM) in particular has stringent requirements for sample thickness, often below 100 nm. In contrast, the ability to tune the X-ray energies offers flexibility in terms of the ability to measure large objects. This Perspective focuses on the use of X-ray techniques as a means to collect chemical information over various time and length scales. It is biased toward techniques that have already seen applicability in battery science. In other words, it is not meant to be an exhaustive review of all X-ray imaging and mapping techniques that may be available. Readers interested in such reviews are referred to several papers in the peer-reviewed literature.<sup>6–9</sup>

## Foreword: Definition of Resolution

Before exploring in detail the different techniques of interest, it is important to define a framework which guides the design of any imaging experiment. This framework is based on the fact that the objective of any chemical imaging experiment is to achieve the maximum resolution along three parameters: space, chemistry and time (as illustrated in figure 3). Because advances in spatial resolution are desirable in order to achieve the ultimate objective of visualizing atomic structures, this parameter tends to be the focus of the attention of researchers developing these techniques. However, as will become apparent throughout this perspective, the deepest level of insight into the electrochemical reactions that determine battery function requires a thorough detection of different chemical states that may often present similar signals, all while operating under an electrochemical stimulus. The latter necessarily implies the importance of temporal resolution so as to acquire multiple data points along the reaction pathway, which may be as fast as seconds. Advances are still needed that push the three parameters forward at the same time. Instead, the current

situation forces sacrifices in either of these scales of resolution.

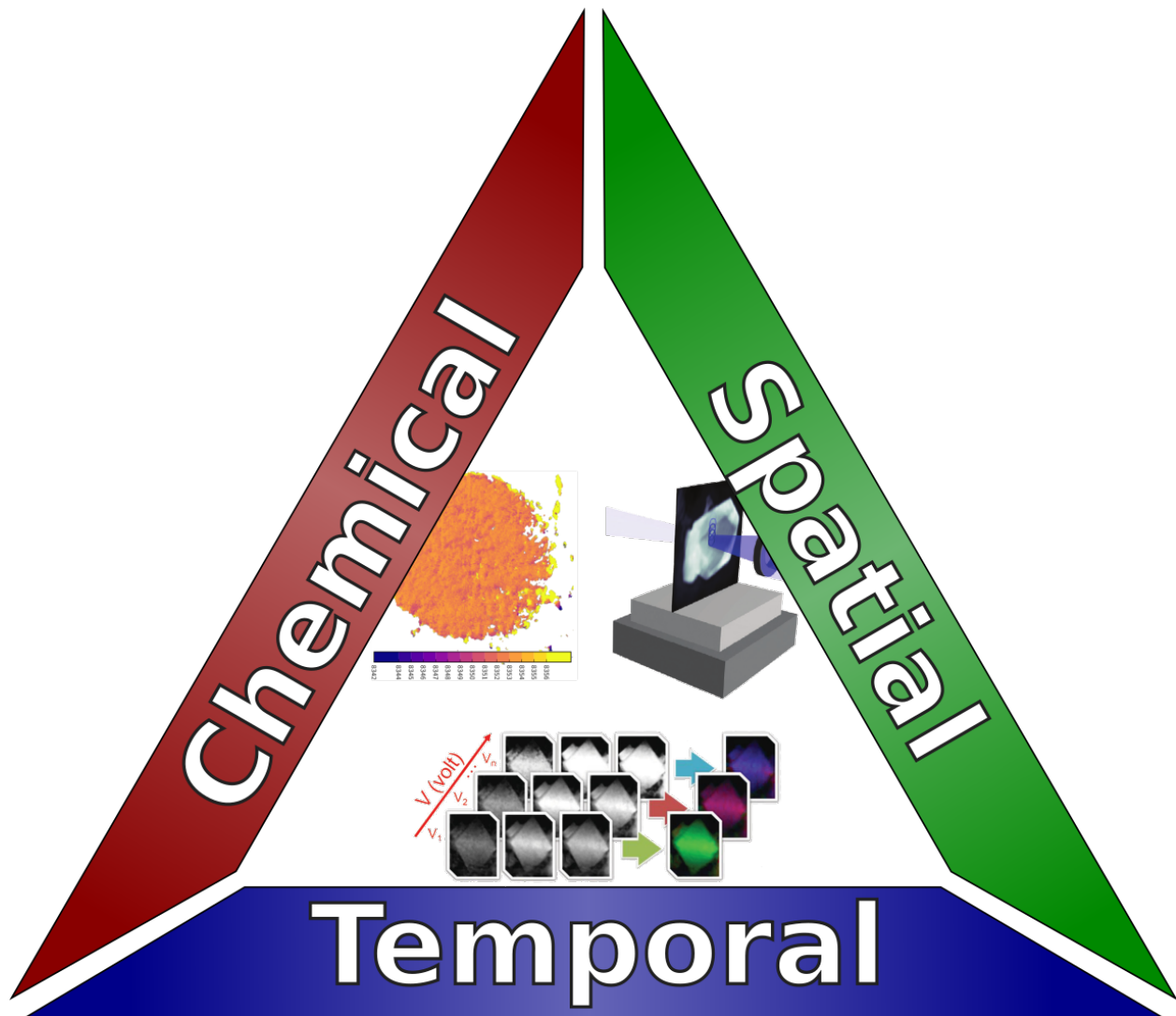


Figure 3: Resolution triangle, showing the trade-off between chemical, spatial and time resolution. Reprinted in part with permission from Yu et al. Nonequilibrium Pathways during Electrochemical Phase Transformations in Single Crystals Revealed by Dynamic Chemical Imaging at Nanoscale Resolution. *Advanced Energy Materials* **2015**, 5. Copyright 2014 John Wiley and Sons. Reprinted in part from reference.<sup>10</sup>

# The X-ray Imaging Experiment

## X-ray Sources

X-ray generation is possible by two different means: laboratory sources and synchrotron facilities. The general concept of the lab source is based on tubes under vacuum, containing a cathode that is biased so as to generate and accelerate electrons. These electrons collide with the metallic anode, generating X-rays over a narrow range of wavelengths. The specific wavelengths of the resultant X-rays are dependent on the metal used for the anode. Common laboratory X-ray sources include the sealed X-ray tube and rotating anode generator, which differ on the level of vacuum, seal and the arrangement of the metallic anode.<sup>11</sup>

Synchrotron radiation is also generated from accelerating charged particles, but provides higher intensity and better coherence than is currently possible with laboratory sources. The particles, typically electrons, are first accelerated to relativistic speeds, at which point they enter the storage ring of the synchrotron. Beamlines are built tangential to the storage ring so as to utilize X-ray radiation generated when the particles are subjected to centripetal acceleration, either through bending magnets or insertion devices, such as wigglers and undulators. Bending magnets serve two purposes. First, they are placed in such a way that the charged particles in the storage ring are redirected to maintain a proper pathway. Second, each redirection generates X-rays, which are then used in experimental stations. Insertion devices are specialized for generating X-rays and differ from bending magnets in that they are straight sections of the ring that have alternating magnetic fields. Charged particles oscillate through the device, with each oscillation essentially equivalent to a single bending magnet. Therefore, the generated photons can reach higher energies than those generated by bending magnets.<sup>12</sup>

An important distinction between laboratory X-ray sources and synchrotron sources is the nature of the X-rays produced. Synchrotron light sources can generate X-rays at much higher intensity than laboratory sources, which can be described in terms of flux and bright-

ness. Flux is representative of the number of X-ray photons that pass a plane per unit time, typically given in photons/second. The definition for brightness varies from author to author, however, the National Institute of Standards and Technology (NIST) defines it as “the radiated power per unit solid angle per unit area normal to the [vector] direction”.<sup>13</sup> To put it simply, brightness is analogous to the flux, while taking into account the source size and divergence. Another major difference between laboratory sources and synchrotron sources is that the optics within a synchrotron create a tunable polychromatic X-ray beam, which can subsequently be set to a narrow energy range through the use of monochromators upstream from the end station. In contrast, laboratory sources only produce a limited range of X-ray energies, which is non-trivial to tune. While some techniques fully utilize the white beam,<sup>14</sup> it is more common to select a single desired wavelength and change it during the experiment. The high flux, brightness and tunability renders synchrotrons as the preferred light sources for chemical imaging.

## Methods of X-ray Microscopy

There are two general modes of X-ray microscopy: full-field and scanning (as illustrated in figure 4). The operation of a full-field X-ray microscope is similar to a conventional visible light microscope. In a full-field microscope, the X-ray beam is first focused down to a few microns. This microbeam illuminates the sample, generating a large frame of view. The resulting photons are magnified by a second set of optics before reaching the detector. In this mode, the limit in spatial resolution is set by the detector pixel size and any aberrations in the optics. This method results in large images with fine resolution in a single shot. In contrast, a scanning microscope is based on focusing the beam prior to illuminating the sample. In order to collect frames of view that are larger than the illuminated spot, the beam is subsequently rastered over the region of interest in the sample. In this case, the spatial resolution is determined by the combination of beam and scanning step size. Given the different methods of operation, it can easily be concluded that full-field imaging offers

higher image throughput than scanning imaging at the highest possible setting. On the other hand, scanning techniques allow for higher versatility in contrast mechanisms than in full field mode, especially when combinations are desired.

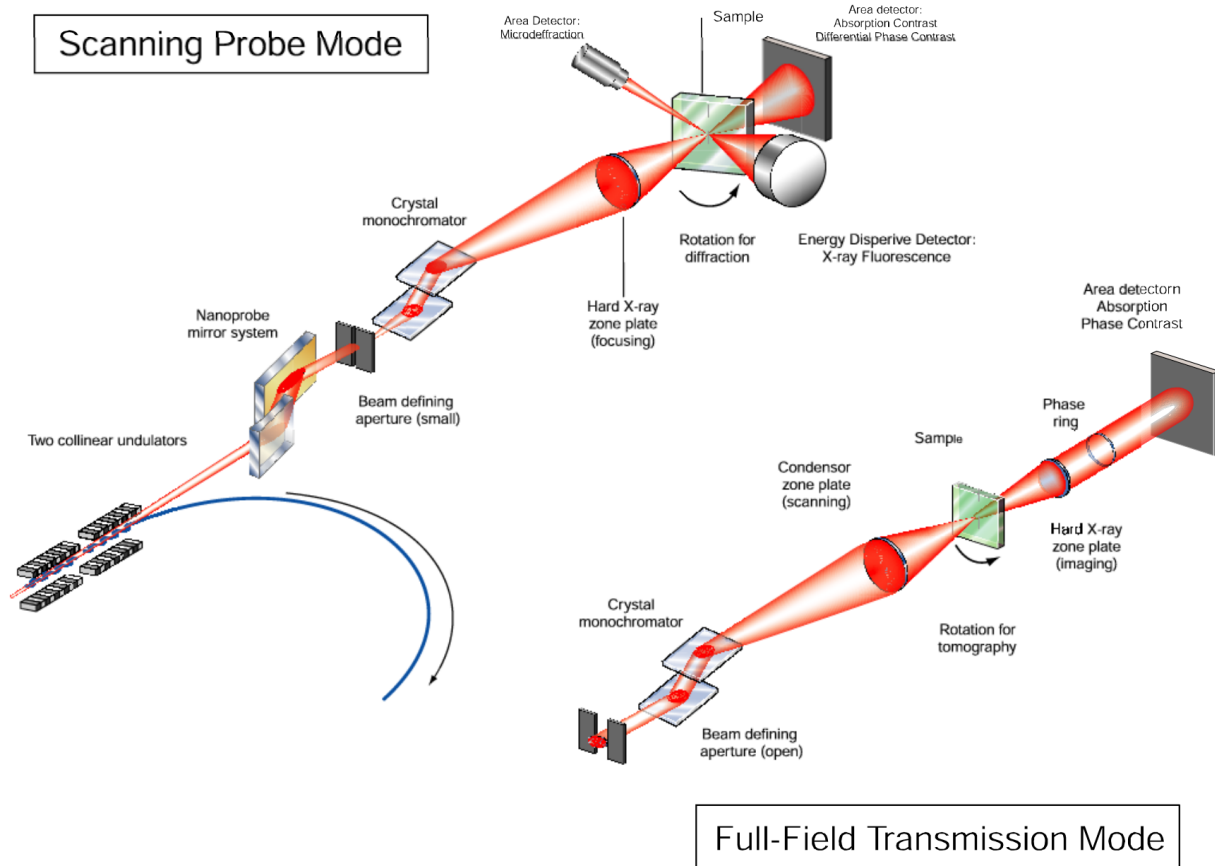


Figure 4: Illustration of experimental configurations for (a) scanning probe and (b) full-field imaging synchrotron hard X-ray microscopy methods. Reprinted with permission from Maser et al. Development of a Hard X-ray Nanoprobe Beamline at the Advanced Photon Source. *Microscopy and Microanalysis* 2005, 11, 680-681. Copyright 2005 Cambridge University Press.

## Tomography

Individual images in both full-field and scanning X-ray microscopes are generated in two spatial dimensions. However, the two techniques offer the capability of 3D imaging using tomography. A tomographic reconstruction is achieved by taking a series of two-dimensional

projection images while the sample is rotated over  $180^\circ$ , followed by conversion of these images to a three-dimensional volume. This process is also known as an inverse Radon transform. This technique is agnostic regarding the contrast mechanism by which the two-dimensional projections were created, meaning it can be combined with any X-ray microscopy contrast mechanism discussed here. Provided the methodology involves the measurement of transmitted photons, tomography allows for the effects of sample thickness to be removed so that the intensity of each voxel is dependent only on material composition. Since the sample is rotating, precise alignment of the rotation axis is necessary to keep the sample in view. There are many algorithms available for performing the reconstruction: each seeks a balance between speed and accuracy. They generally fall into two categories: analytical and iterative. Analytical techniques are usually a variant of back-projection and vary by the exact nature of the filters applied to the input data. They have the advantage of being very fast, but often introduce artifacts. Iterative techniques introduce fewer artifacts that also tend to be uncorrelated, but reconstruction often requires many iterations to achieve reliable results, which makes this approach considerably slower than the analytical algorithms. New methods are being developed that combine the advantages of both techniques. For example, if many samples with similar properties are to be analyzed, a set of optimized filters for back-projection can be derived via machine learning. The initial training is quite slow but once complete, the filters can be used with any new dataset provided that the sample responds similarly to the training data.<sup>15</sup> However, this requirement is stricter than it seems at first sight: many of the desired insights about an electrochemical reaction depend on the precise measurement of changes in the interactions between material and X-rays during the experiment. A major advantage of this approach, though, is that the training can be performed in such a way that it expects low quality datasets, such as those with few projections, so subsequent experiments have increased temporal resolution.

## X-ray Optics

All the techniques discussed here require at least some level of focusing of the X-ray beam prior to, and, in some cases, also after, interaction with the sample. The ability to obtain images at increasing spatial resolution is dependent on the type, sophistication and quality of the focusing optics.

Compound refractive lenses (CRL) use several lenses in series to focus an X-ray beam. CRLs are made of low atomic number materials to reduce X-ray absorption.<sup>16</sup> Reflective optics are used as well for X-ray focusing. First proposed by Kirkpatrick and Baez in 1948, one common setup is the use of two grazing incidence reflective mirrors that are orthogonal to one another (KB mirrors). This setup allows for the incoming X-ray beam to be focused in both dimensions. Both CRLs and KB mirrors are typically used for hard X-rays.<sup>17</sup>

Diffractive optics are an alternative option. They are predominant in the soft X-ray regime, but are also compatible with hard X-ray radiation. Fresnel Zone Plates (FZP) utilize several concentric rings of alternating opaque and transparent zones, decreasing in width as a function of distance from the center. In this way, the diffracted X-rays from the transparent sections of the optic will undergo constructive interference, focusing to a point. The maximum amount that the beam can be focused is inversely related to the width of the outermost ring. Multi-layer Laue Lenses (MLL) are similar to FZPs, in that they use zones to achieve focusing. However, MLLs use one-dimensional zones rather than rings. Because of this, they can be synthesized using thin film deposition, which allows for smaller thicknesses than current lithographic techniques.<sup>12,18</sup>

Modern focusing optics typically limit the spatial resolution of the measurement to roughly 10 nm, with MLLs.<sup>19</sup> Focusing optics have an inherent disadvantage that the resultant spatial resolution is dependent on the optic itself. Lensless techniques remove this restriction. Coherent diffraction patterns may be collected and processed using an iterative reconstruction method to produce an image. Thus, the ultimate limit resides in the wavelength of the incoming radiation, also known as the diffraction limit, meaning that spatial

resolutions can be achieved that are smaller than the size of the beam on the sample and the nominal resolution of the optics. Techniques derived from this approach are further discussed below.

## Detectors

In general, X-ray detectors fall into two categories: integrating and counting. Integrating detectors store up the total number of photons and are periodically read and cleared by the electronics. In contrast, counting detectors register and report each individual photon captured as a separate event. Detectors of the same operating mode share common properties, even if the underlying mechanisms may vary significantly. Integrating detectors usually have a limit on how many photons they can capture before being read, which effectively limits the dynamic range. Counting detectors do not have this limitation. However, there is a certain dead-time involved in converting the photon into a digital signal and any other photons arriving during this time will not be detected. It is worth noting that the first detectors were actually two-dimensional analog film, though they have been superseded by digital detectors, either charge-coupled device (CCD), multi-wire proportional counters (MWP), or arrays of point-detectors. CCDs are integrating detectors and, as such, respond well to high flux/count rates since there is no dead-time associated with each photon event. A proportional counter detects each photon as a separate event so there is theoretically no limit to its dynamic range other than the bit-depth of the downstream electronics. In an MWP detector, each photon induces an avalanche of ionization near the detector anode, which is then neutralized when the charge drifts back towards the cathode. This reset time limits the local flux that can be measured accurately. Combined with the time needed for readout of each event, this limits the global flux that can be measured accurately. Proportional counters are more common on laboratory instruments, whereas CCDs dominate in synchrotron experiments.

In full-field microscopy, the magnified X-ray image strikes a scintillator where it is converted to visible light. The total energy of this conversion must be conserved, so one high-

energy X-ray photon results in hundreds of low-energy visible light photons. This light is then magnified using visible-light microscopy optics onto a detector, usually a CCD. Any defects in the scintillator are clearly visible in the resulting intensity images so it is important to collect a reference frame to remove these features. For scanning microscopy, no post-sample optics are required. Instead, a detector measures the transmitted intensity at each raster position. Photomultiplier tubes (PMTs) have a large collection area, low noise and high gain, making them ideal for this application. In some specific scanning microscopy methods, a two-dimensional interference pattern is needed at each raster position, so a CCD detector is used instead.

Detectors specific for the detection of diffracted X-rays can also be described by their geometry. Point-detectors can capture photons at only one position at a time and are then scanned across a range of scattering angles to acquire a one-dimensional diffraction pattern. They are commonly used in laboratory diffractometers and when the sample can be assumed to behave as an ideal powder. A major advantage is that a variety of absorbers and slits can be positioned to reduce fluorescence and air scattering. Line-detectors can capture a range of angles simultaneously. They produce the same one-dimensional pattern, only faster. A disadvantage of both of these geometries is that they only retrieve a slice through the full Debye-Scherrer rings. If only a small number of crystallites are present, it is unlikely that any diffraction conditions will land on this slice. For diffraction mapping techniques this is often the case, so these detectors are unsuitable. An area detector, however, captures a two-dimensional segment of the full pattern and so any diffraction vectors landing within this segment will be detected. The exact range depends on the geometry of the experimental setup and the wavelength of radiation used: high energy X-rays cause more diffraction conditions to be detectable in a given area. A 1-dimensional diffraction pattern can then be obtained by integrating across the Debye-Scherrer rings.

The dynamic range of the detector is an important factor to consider. CCDs work by exposing a photo-active layer to radiation, which then results in charge accumulation in the

underlying structure, to be read out after some time interval. If a single CCD pixel becomes saturated before being read, any additional charge from subsequent photons will bleed into neighboring pixels. In full-field microscopy, this tends to be a problem in the reference images, since the maximum intensity is larger: these areas will have artificially low values in the resulting optical depth image. Shortening exposure time can solve this problem, however the resulting data will have a lower signal-to-noise ratio. A simple solution is to keep the exposure time short and then collect and average multiple frames.

## Mechanisms of Chemical Contrast

### Hyperspectral Imaging

X-ray microscopy utilizes a multitude of contrast mechanisms. *Absorption contrast* relies on the intensity of the X-rays that penetrate through the material being imaged. From the physical perspective, it involves detecting changes in the amplitude of the incoming X-ray wave after interacting with the sample. Most commonly, the changes are detected after transmission of the X-ray beam through the sample. Thickness and composition of the material are two major contributing factors to the X-ray absorption. Therefore, through the collection of one signal, both morphological and chemical information can be generated. Since X-ray absorbance depends on interaction with electrons, elements with higher atomic numbers have a higher absorbance. The transmitted intensity drops exponentially with increasing penetration length, so it is more convenient to express this value as a logarithm of the ratio of incident radiation that is actually transmitted; the resulting absorbance value scales linearly with sample thickness provided the material is homogeneous. Two-dimensional imaging of heterogeneous samples requires a more sophisticated interpretation since thickness and composition both affect the absorbance. Once the X-ray energy exceeds that needed to promote a core electron, a sharp increase in X-ray absorbance is seen, known as an edge. At these energies, core electrons are excited either to the unbound continuum or

to higher energy unoccupied states as allowed by selection rules. Therefore, the specific energy value of the transition is indicative of the element and its chemical state (eg. formal valence state). Each element can potentially have several absorption edges, depending on how many core electron orbitals it has. These edges are named based on the electron energy level they originate from: “K-edge” for  $n = 1$ , “L-edge” for  $n = 2$ , “M-edge” for  $n = 3$ , etc. A typical K-edge spectrum consists of two regions, XANES (X-ray absorption near-edge structure) and EXAFS (extended X-ray absorption fine structure). XANES provides information on oxidation states while EXAFS provides information on local atomic structure and neighboring atoms. In practice, collection of EXAFS data imposes data acquisition requirements that are currently unrealistic in spectromicroscopy. Since the oxidation state of transition metals is of primary interest in battery materials, K-edge spectra of these elements are a very common target for this technique. The L-edge spectrum of an element contains information regarding the molecular orbitals associated with its atoms, and, as a result, is also of interest in spectromicroscopy.

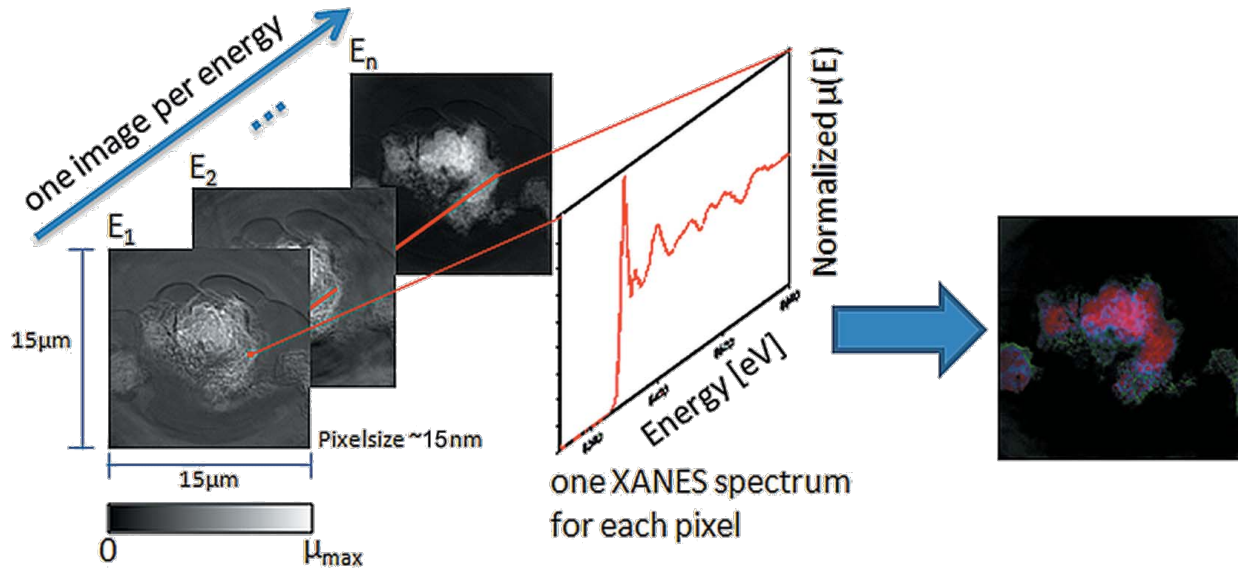


Figure 5: Reduction of TXM stacks to form chemical maps. A full spectrum is extracted for each pixel and used to calculate the chemical state of the material and then converted to a color.<sup>20</sup> Reproduced with permission of the International Union of Crystallography.

*Fluorescence contrast* is similar to X-ray absorption in that it relies on electron excitation.

The fluorescence signal, however comes from the subsequent light re-emission. For the element of interest, the X-ray energy can be set just above the absorption edge. If the incoming X-ray energy is set above the absorption edge for several elements of interest in a sample, they will all fluoresce at different energies. Thus, fluorescence imaging can be advantageous over X-ray absorption for gathering elemental distribution, especially in dilute samples. If the energy is scanned below and through the edge, fluorescence detectors can also be used to produce X-ray absorption spectra, in a manner that is compatible with spectromicroscopy. This approach was recently demonstrated in battery materials.<sup>21</sup>

An alternative to imaging of absorbance events, *phase contrast* imaging monitors the changes of the observed phase of X-ray waves, as opposed to their amplitude, denoted by the phase shift term,  $\delta$ . These changes are observed as the thickness/density of the sample changes. In order to resolve the observed differences in the phase shift the detector used must be placed at a sufficient distance away from the sample. This distance can vary from technique to technique; 0.9 m has been reported for coherent diffractive imaging (a specialized mode of phase contrast imaging described more fully below),<sup>22</sup> while 108 cm has been reported for a more traditional experiment.<sup>23</sup> Phase contrast imaging is advantageous as it is more sensitive than absorption contrast, and can therefore utilize lower X-ray energies. Therefore, this technique is often used to study materials that do not absorb strongly or materials sensitive to radiation damage caused by high energy X-rays. A drawback for some, phase contrast imaging heavily relies upon a highly coherent X-ray source, as well as a sophisticated detector. A full complex refractive index can be acquired using phase contrast, by collecting data over a range of energy points. This information will also be dependent on the electronic structure of the sample.

In spectromicroscopy, whether full-field or scanning, the same field-of-view is imaged repeatedly while the energy of the incident beam is changed over an absorption edge of the element(s) of interest. The change in phase contrast with X-ray energy can also be measured to produce chemical information.<sup>24</sup> However, this approach is still currently under

development, partly because correlation between spectra and chemical information remains to be fully established. The resulting frame-stack provides a full absorbance and/or phase spectrum at each pixel. These spectra are then processed into a scientifically meaningful quantity to generate chemical maps of the field-of-view. In order for pixel-wise spectroscopic conclusions to be valid, it is critical that the images are properly aligned with one another, which is rarely the case with raw datasets. To correct for these inconsistencies, some form of image registration is usually necessary. The next step in the analysis involves normalization of the spectra relative to the background optical depth. As X-ray energy increases, the transmission of all materials increases as well. Correcting for this effect improves the reliability of analysis methods that involve decomposing the spectra into components of known materials.<sup>25</sup> Conversion of the resulting absorbance spectra to some figure of scientific merit depends in large part on the question being addressed by the experiment. A common goal is to map the distribution of certain elements. This goal can be accomplished by collecting two frames per element: one above and one below the absorption K-edge. By comparing these “edge-jump” values for the elements in question, their relative concentrations can be calculated.<sup>26</sup> Alternatively, generating spectroscopic maps involves reshaping the data to give an array of spectra, each one corresponding to a pixel in the final map. This outcome is accomplished by “looking through” a frame-set along the energy dimension and flattening along the image dimensions, as illustrated in figure 5. In theory, any analysis that is performed on a bulk spectrum can be done on a single-pixel spectrum. In practice, there are generally a lot of spectra to be analyzed; a set of  $1024 \times 1024$  frames contains over 1 million spectra to be processed. This situation means that analysis cannot rely on human intervention. If prior knowledge of the presence and distinct spectra of multiple phases in the dataset is available, their signals can be decomposed.<sup>10,27,28</sup> If the component spectra are not known, which is often the case, a variety of signal processing techniques, such as *independent components analysis* (ICA)<sup>29</sup> or *Bayesian* methods,<sup>30</sup> can be used to approximate them and extract the relative proportions of each component.<sup>31,32</sup> Care must be taken, however,

since many of these methods assume properties of the data that are not necessarily true. *Principal components analysis* is a common alternative to ICA that has seen application in spectromicroscopy of battery materials.<sup>10,33</sup> Another approach involves the use of numerical methods to directly map some property of the spectrum. This approach is most effective if an argument can be made that the directly calculated value correlates strongly with some change in the properties or state of the material. For example, the oxidation state of nickel in several layered battery cathode materials is accompanied by a shift in the edge and whiteline positions of the corresponding K-edge spectrum to higher energies;<sup>34</sup> extracting and mapping the whiteline position for each pixel's spectrum can provide a map that approximates the oxidation state of the metal and consequently the state-of-charge of the material. Care must be taken to account for small variations in absorbance across the two or three largest absorbance points which are not due to the sample, but background or spurious signals.

## Bragg Diffraction Microscopy

Bragg X-ray diffraction (XRD) provides complementary information to spectroscopy. Rather than observing electronic transitions, it provides a measurement of the distance between crystalline planes (d-space) within a material. This crystallographic information means that unit cell parameters, atomic defects, strain and microstructural information of the coherent domains are available. Of particular interest in the context of this discussion is the ability to interpret the unit cell dimensions as a given chemical composition if prior knowledge of the system exists. In order to observe diffraction from a material, the Bragg condition must be satisfied, in which a particular X-ray wavelength, crystal spacing, and orientation must be met. A conventional XRD experiment holds the X-ray wavelength constant, while altering the incident and detected beam angles. In contrast, energy dispersive X-ray diffraction (EDXRD) holds the orientation constant and varies the wavelength. As a result, no goniometer is required and the variation in wavelength can be used to profile the depth of the sample, but extracting physical quantities from the resulting data is less

straightforward.<sup>35,36</sup> Once a diffraction pattern is obtained, crystallographic parameters can be extracted and used for mapping. The data generated in Bragg diffraction microscopy experiments can be treated very similarly to those collected during spectromicroscopy. Each mapping position is equivalent to a pixel in an X-ray micrograph and a series of frames are collected at different scattering vectors,  $q$ . Generally, the spatial dimensions are the slowest-changing in diffraction mapping, whereas they are the fastest (or even simultaneous) in microscopy; this distinction does not change the structure of the data in a significant way. However, it does obviate the need to align each image. Rather than a full absorbance spectrum at each location, these experiments generate a diffractogram at each position. Theoretically, a researcher can analyze the two-diffraction pattern at each position; often, the 2D patterns are integrated to form the more traditional 1D diffractograms. From here, a refinement can retrieve crystallographic parameters, such as unit-cell dimensions, strain or phase ratios.

## The Ultimate Frontier: The Lensless Microscope

A technique that uses phase contrast imaging in conjunction with Bragg diffraction is coherent diffractive imaging (CDI). A single particle fulfilling the Bragg condition is illuminated by a coherent X-ray beam that is larger than the particle. The detector is placed far away from the sample, so that it can collect fringes of the diffracted beam. An iterative algorithm is used to reconstruct an image from the phase information in the fringes of a three-dimensional diffraction pattern.<sup>37</sup>

Ptychography is another lensless technique which also relies on collecting the full diffraction pattern using coherent diffraction. Unlike CDI, this is a scanning technique; small spots are collected in such a fashion that they spatially overlap on the sample. Similar to CDI, ptychography utilizes an iterative algorithm to reconstruct an image from the diffraction patterns. A random object image is first generated. For each scanning position, a Fourier transform is performed on the object and is convolved by the illumination probe. The real

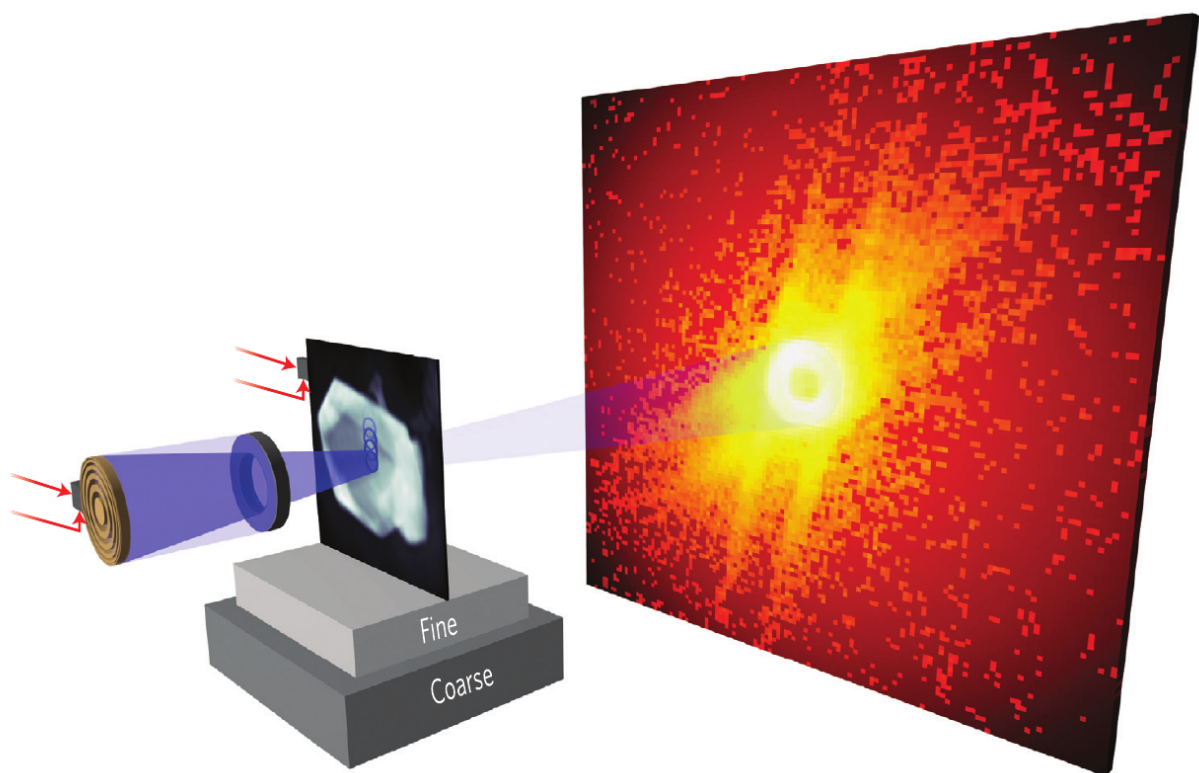


Figure 6: Schematic of soft X-ray ptychographic microscope. An incoming X-ray beam is focused onto the sample by a zone plate and order sorting aperture. The coherent diffraction pattern is collected by a CCD.<sup>10</sup>

component is replaced by the recorded interference pattern and an inverse Fourier transform is then done to recover an improved object. This procedure is carried out for each scanning position and then repeated until a solution converges. As a result, the ultimate spatial resolution is, to a large extent, independent from the size of the beam used to collect the overlapping patterns. In other words, as a lensless technique, the process of generation of images does not suffer from lens aberration and thus allows for very high spatial resolution approaching the diffraction limit, under 10 nm in some cases. Artifacts from the reconstruction process sometimes manifest as high frequency bands alongside sharp edges in the specimen. Since this technique is driven by an interference pattern, the best reconstructions are obtained from strongly scattering materials. Ptychography has also been performed in tomographic mode,<sup>38</sup> but this methodological area is still in its infancy. As an added bonus, the reconstruction produces both the real and imaginary components of the object image. By comparison to an area with no material, the fully complex refractive index can be calculated. Exploiting the complex-valued nature of this technique is a relatively unexplored area.

## Visualization and Colormaps

Turning a large dataset into a two-dimensional image is a task that becomes more challenging as the number of dimensions increases. For applications with two spatial dimensions, map images are generated by data-reduction as described in the preceding sections. The relationship between values and colors is known as a “colormap” or “lookup table”. The choice of colormap can have subtle effects on how the data are interpreted. In general, human vision associates the brightness of a color with the value it represents, regardless of its hue. Therefore, an effective colormap translates high values to high-brightness colors and low values to low-brightness colors. Rainbow colormaps, such as *jet*, do not meet this criterion and should be avoided for representing sequential data. *Jet* contains bands of high and low brightness that are perceived as sharp gradients in the data that do not actually exist. Perceptually

uniform colormaps, such as *viridis* for Matplotlib and *parula* for Matlab, are designed to avoid this problem. Additionally, *viridis* was tested against color blindness and ensures that data display properly to people in this category.

Projecting data with three spatial dimensions onto a two-dimensional canvas can be done with any one of several visualization tools. Typically, certain features in the data are of interest, such as internal fractures within particles or the distribution of certain elements. Successful visualization usually requires additional analysis steps that identify and highlight these features while making the surrounding material partially transparent. Avizo (FEI) is a popular commercial software package specifically designed to work with tomography data: it contains a number of filters that allow the data analysis to be performed within one piece of software. An additional Avizo package can be purchased that allows it to handle datasets that do not fit entirely into main memory, which is often the case for tomography. An alternative is Paraview (Kitware Inc. and Los Alamos National Lab), a general purpose visualization platform that is highly extensible, allowing python plugins to be run from within the application. Paraview has the additional benefit of being free and open source. For quick inspection of tomographic slices, ImageJ provides the Volume Viewer plugin (included in the FIJI distribution), which is more straight-forward to use than either Avizo or Paraview, but has fewer features.

## Ex situ versus operando

To a large extent, electrochemistry is most interesting when away from equilibrium. As electrochemical devices, batteries are useful during operation, which is inherently under kinetic control. While the kinetic states are determined by the thermodynamics of the system, metastability is more prominent under electrochemical conditions than in other classical chemical environments, such as high temperatures. This prominence also implies that the probability of producing kinetic states that are only weakly metastable is high.

In fact, the problem of self-discharge, common in certain batteries, is precisely the product of equilibration of a metastable charged state. As a consequence of the pervasive kinetic control, ex situ measurements, which rely on harvesting samples from a cell at a desired chemical state, introduce uncertainty when the goal is to describe relevant states under working conditions. Nonetheless, if caution is applied, and due to their simplicity, these measurements can still provide valuable guidance,<sup>28</sup> mainly because they do not critically suffer from constraints in measurement time and, thus, can result in the highest data quality. Ultimately, operando measurements of battery reactions are preferred because of the growing body of evidence showing that there are many cases where the state within an operating battery is different from what is observed once the cell is disassembled,<sup>39,40</sup> especially when high rates are employed. For this reason, researchers developing novel methods of imaging should have motivation to enter a path that results in means to operando analysis. At this point, given certain confusion in the field, it is worth clarifying that we consider operando measurements to be a small subset of in situ science. The condition sine qua non for an operando

experiment is that the cell is not stopped to collect data unless the goal is specifically to measure equilibration phenomena.

While operando measurements are preferred and should be pursued, they can present several challenges of varying degrees of difficulty. The setup must allow photons to pass through both the sample and apparatus with very little disturbance to the signal from the apparatus itself. First and foremost, X-ray absorbing materials have to be minimized in order to ensure sufficient signal reaches the detector. Ideally, supporting materials containing heavier elements should be removed, or made sufficiently thin so as to minimize their effects. Another challenge is avoiding X-ray induced damage to supporting materials, such as the polymer binder often used in the construction of cathodes. Maintaining adequate stack pressure may also be important, depending on the nature of the experiment.<sup>41</sup> Additionally, the possibility of deleterious effects of X-ray exposure on the behavior of cathode materials

is not completely understood. One possibility is to use very high energy X-rays, which can penetrate the casing material<sup>42</sup> and are less damaging. This strategy is valid for some diffraction experiments, but cannot be applied to spectroscopic imaging since specific energies at which the X-ray beam is absorbed are required.

In situations where high-energy X-rays are not possible, a transparent window is necessary. Beryllium is a typical choice, but its use introduces stringent handling requirements due to its high toxicity, especially in the dispersible form that is generated, for instance, during machining. It also oxidizes relatively easily, making it unsuitable for high-voltage battery applications. Silicon nitride is an appealing option since it can be purchased commercially in prefabricated windows down to tens of nanometers in thickness. At these thicknesses, it also does not have any noticeable morphological features, making it suitable for X-ray microscopy techniques. However, they are very fragile due to their thickness. Polyimide (Kapton) film has found widespread use in operando diffraction experiments, despite the fact that it also introduces an amorphous contribution to diffraction patterns. It has relatively high transmissivity, is easy to fabricate and is chemically inert. Unfortunately, it cannot ensure a complete seal and, like many other plastics, it often contains filler particles which are heavy enough to become visible in a microscopy experiment, interfering with observations and, thus, rendering it unsuitable. Amorphous carbon can also be used. A large advantage here is its electrical conductivity, which eliminates issues of electrochemical inactivity of the material behind the window. Since it is made entirely of carbon, it also interacts only very weakly with X-rays, so it induces minimal signal attenuation. However, it is difficult to fabricate, and can react under certain conditions, such as at very high potentials or against lithium metal. The AMPIX electrochemical cell, developed by Argonne National Laboratory, is an example of a cell with amorphous carbon windows that fits the requirements of an operando X-ray experiment. The cell design ensures good stack pressure as well as electrical conductivity, closely mirroring coin cell conditions.<sup>41,43</sup> Even more sophisticated cells are needed when using low energy, soft X-rays, where the sample volume

must be small to avoid excessive absorption of the signal by the sample. In this case, designs that rely on microfabrication have recently been demonstrated.<sup>40</sup>

Operando measurements create the most severe challenges to an imaging experiment when considering the three scales of resolution above, namely spatial, chemical and temporal. Many battery reactions span several hours, but the need to build a reaction pathway means that it is desirable to collect at least 5 data points during the reaction. This goal imposes restrictions on the time available to complete an image containing the desired chemical information, at the desired level of spatial resolution. Unfortunately, all modes of chemical contrast require collecting multiple frames for the same reaction state to reconstruct a map of the species present in the field view. Using XANES microscopy as an example, chemical resolution is achieved by collecting frames at a large number of energies, with the limit being set by the precision of the upstream optics. In the particular case of scanning techniques, spatial resolution requires the use of the smallest possible step size to raster the field of view, meaning that a similar trade-off emerges in that the acquisition time is directly affected by this parameter. Additionally, increasing the collection time for each frame will improve the signal-to-noise ratio and improve the accuracy of the data, again at the expense of longer acquisition times for a full frame-set. In practice, the most common choice is to minimize the number of points to obtain some level of chemical resolution in the individual frame-set, whether scanning energy (spectroscopy) or a beam-sample-detector angle (diffraction). This approach strongly relies on prior knowledge of the chemical species involved during the reaction, so that energies or angles are chosen at which signals between these species differ the most. Such prior knowledge is typically acquired through XAS or XRD measurements of the bulk average, as opposed to spatially resolved regions. In the case of the spectroscopy of transition metal species, a change of one unit in the formal oxidation state translates into a displacement of the signals of a few electron-volts, which renders the method viable. Challenges arise when the changes between species are small, for instance, when compounds exist at redox states intermediate between end members. The strategy also inherently lends

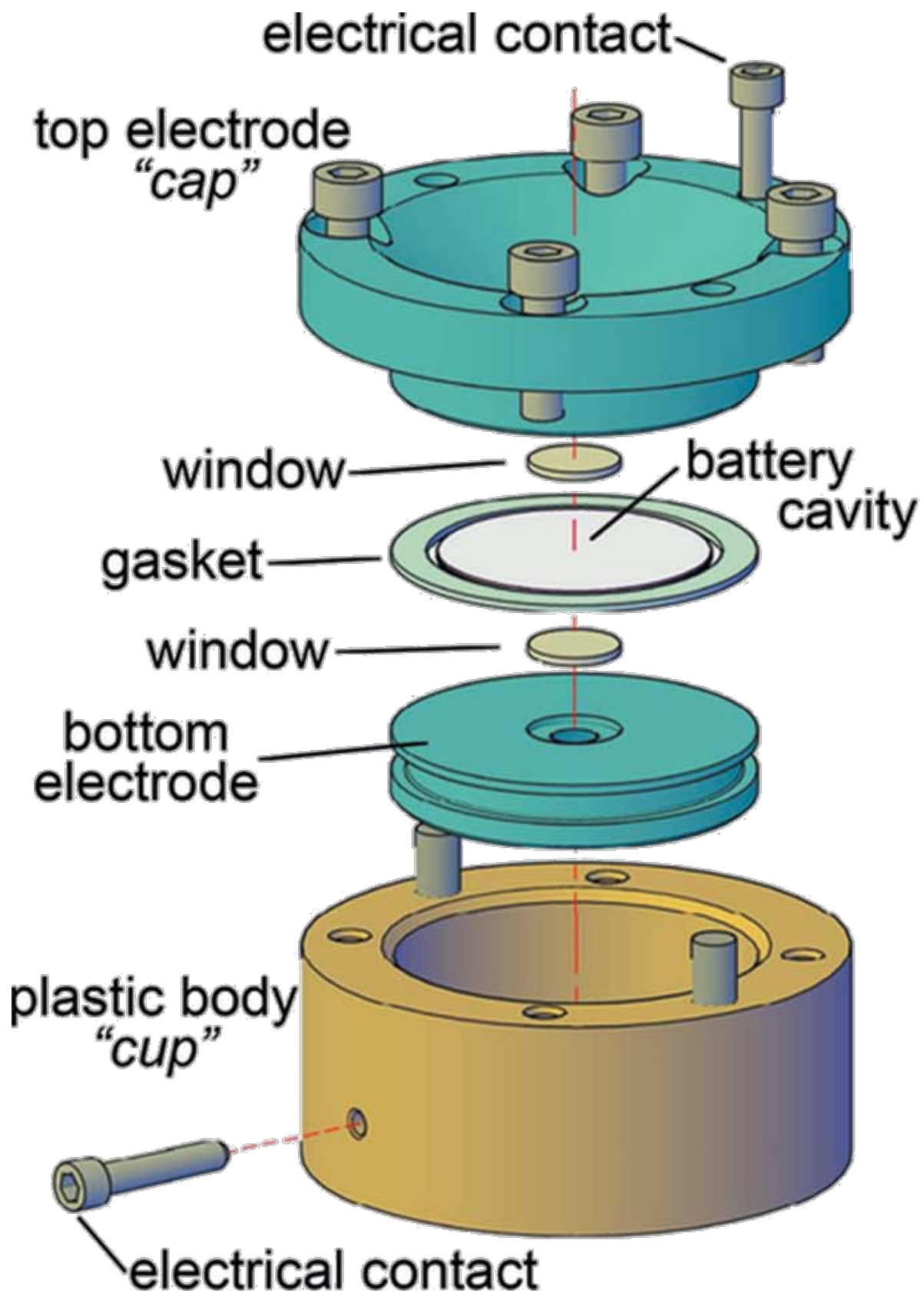


Figure 7: Schematic of AMPIX electrochemical cell.<sup>43</sup> Reproduced with permission of the International Union of Crystallography.

itself to misinterpretation if previously unknown or unexpected states form in the measurement, especially if they are related to the known, expected species. The local character of an imaging measurement means that the limit of detection of minority species increases with respect to a data set gathered from the bulk average, especially if they accumulated in specific regions of the image. All in all, it is important to be aware of the compromises made to avoid over-analyzing data. Since the field of X-ray imaging is vibrant and constantly pushing the boundaries in resolution, it is likely that these limitations will be alleviated with time, creating exciting opportunities for rich insight into battery operating conditions.

## Applications of X-Ray Imaging to Problems in Battery Research

In this section, we describe case studies that highlight the power and versatility of X-ray imaging to elucidate phenomena occurring in battery materials. As a result, this section is not meant to be exhaustive. We mostly focus on examples of electrode materials containing transition metals, as they are the most pervasive in the literature. The specifics of each material are not discussed beyond their chemical identity and a brief mention of the insight gained by imaging. For an extensive discussion of the current body of knowledge of electrochemical reactions in the battery materials discussed here, the reader is referred again to reviews existing in the literature.<sup>44,45</sup>

Absorption imaging at a single X-ray energy provides a direct look at the internal morphology of the material. The short acquisition times and relatively straightforward technical requirements mean that high temporal resolutions can be achieved. Tomography is also common. 3D morphological imaging can even be achieved with laboratory X-ray microscopes.<sup>46</sup> Despite the lack of direct chemical contrast, this type of experiment can still illuminate details of the underlying mechanism. One example involves novel use of a heat-transfer model to extract tortuosity and porosity data from three dimensional electrode volumes.

This experiment revealed significant anisotropy and heterogeneity in pore structure, with implications for modeling electrode behavior.<sup>47</sup>

Several experiments in battery research highlight the ability of X-ray imaging to track the distributions of specific elements. Migration of transition metals after one cycle was seen by X-ray absorption tomography.<sup>48</sup> Specifically, the authors discovered depletion of the transition metals at the surface of the particle, accompanied by manganese segregation. Another example used this technique to track transition metal distribution across multiple cycles in a particle of mixed transition metal oxide  $\text{LiNi}_{0.4}\text{Mn}_{0.4}\text{Co}_{0.2}\text{O}_2$ .<sup>49</sup> The authors showed an excess of manganese and a depletion of cobalt and nickel at the surface of the particles when using specially designed materials. It is known that an irreversible conversion of nickel to a reduced rock-salt phase occurs at the surfaces in these materials. This low cobalt/nickel material shows a subsequent improvement in high-voltage electrochemical cycling performance.

Insight can be gathered from techniques that are currently optimized for ex situ experiments. Hard X-ray full field microscopy has seen rather broad applicability to questions in battery research. It has effectively been demonstrated to locate delithiation domains in olivine-type  $\text{LiFePO}_4$  microcrystals, and subsequent morphological events, such as fracture were identified.<sup>33</sup> However, the spatial resolution of a hard TXM,  $\sim 30\text{ nm}$ , did not allow for a specific correlation between chemical domains and fracture points. To achieve this knowledge, soft X-ray absorption spectroscopy coupled with ptychographic microscopy was required in order to gather information at the highest spatial resolution possible today. Yu et al. investigated how crystal size impacts the transformation of  $\text{LiFePO}_4$  to  $\text{FePO}_4$ .<sup>28</sup> Chemical maps were successfully produced for particles ranging from  $<100\text{ nm}$  to several microns in length. The high spatial resolution achieved in these ptychography measurements,  $\sim 10\text{ nm}$ , finally revealed the correlation between chemical stats and physical artifacts, such as cracks. Indeed, comparison of ptychographic imaging with conventional scanning spectromicroscopy revealed an increase in the sharpness of the images, making such spatial correlation was

possible. Panels a and b of figure 8 highlight the extent of improvement.<sup>10</sup> The work demonstrated that reducing the size of LiFePO<sub>4</sub> particles resulted in less extensive fracturing while the distribution of reaction products was very similar, which was taken as an indication of the superior electrochemical performance from LiFePO<sub>4</sub> nanoparticles.<sup>28</sup>

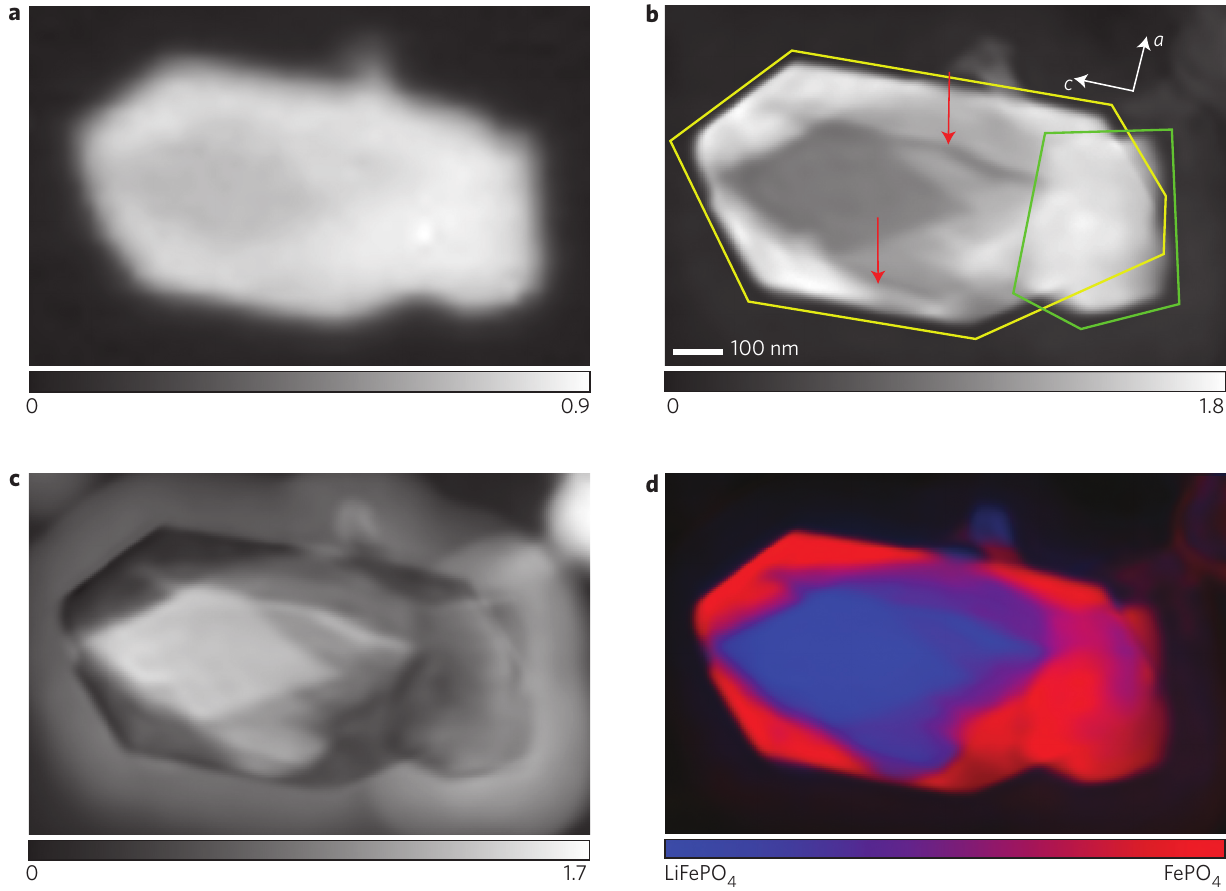


Figure 8: (a), (b) X-ray microscopy of partially delithiated LiFePO<sub>4</sub>. Optical density maps from STXM (a) and ptychography (b) at 710 eV, showing maximum absorption contrast between the end members. The spatial resolution of the STXM is not adequate to visualize the presence of multiple particles, which are outlined in the ptychographic image, and cracks along the crystallographic c axis, which are indicated by red arrows (the a and c crystallographic axes are indicated by white arrows; the b axis is parallel to the X-ray transmission). (c) Phase of the ptychographic reconstruction at 709.2 eV, showing maximum relative phase shift between the end members. The halo around the particle is carbon contamination. (d) Colorized composition map calculated by principal component analysis, clustering and singular value decomposition of the full complex refractive index.<sup>10</sup>

Little work has been done on diffraction mapping of lithium-ion cathodes. The most well-known example comes from Liu et al.,<sup>50</sup> where the authors used synchrotron radiation to map

the surface of an electrode recovered from a partially charged prismatic cell. However, this work was carried out at coarse spatial resolutions, of several  $\mu\text{m}$ , compared to the nanoscale insight of other microscopic mechanisms discussed in this Perspective. Nonetheless, valuable information was gathered at the scale of the whole electrode. Indeed, at high rates, they found a strong gradient in the phase distribution along the direction of current flow from the connector tab. The choice of a two-phase material ( $\text{LiFePO}_4$ ) means the phase distribution within a large electrode is unlikely to change dramatically once the driving force is removed and the electrode is removed from the cell, and, thus, meant that the ex situ measurements produced meaningful data

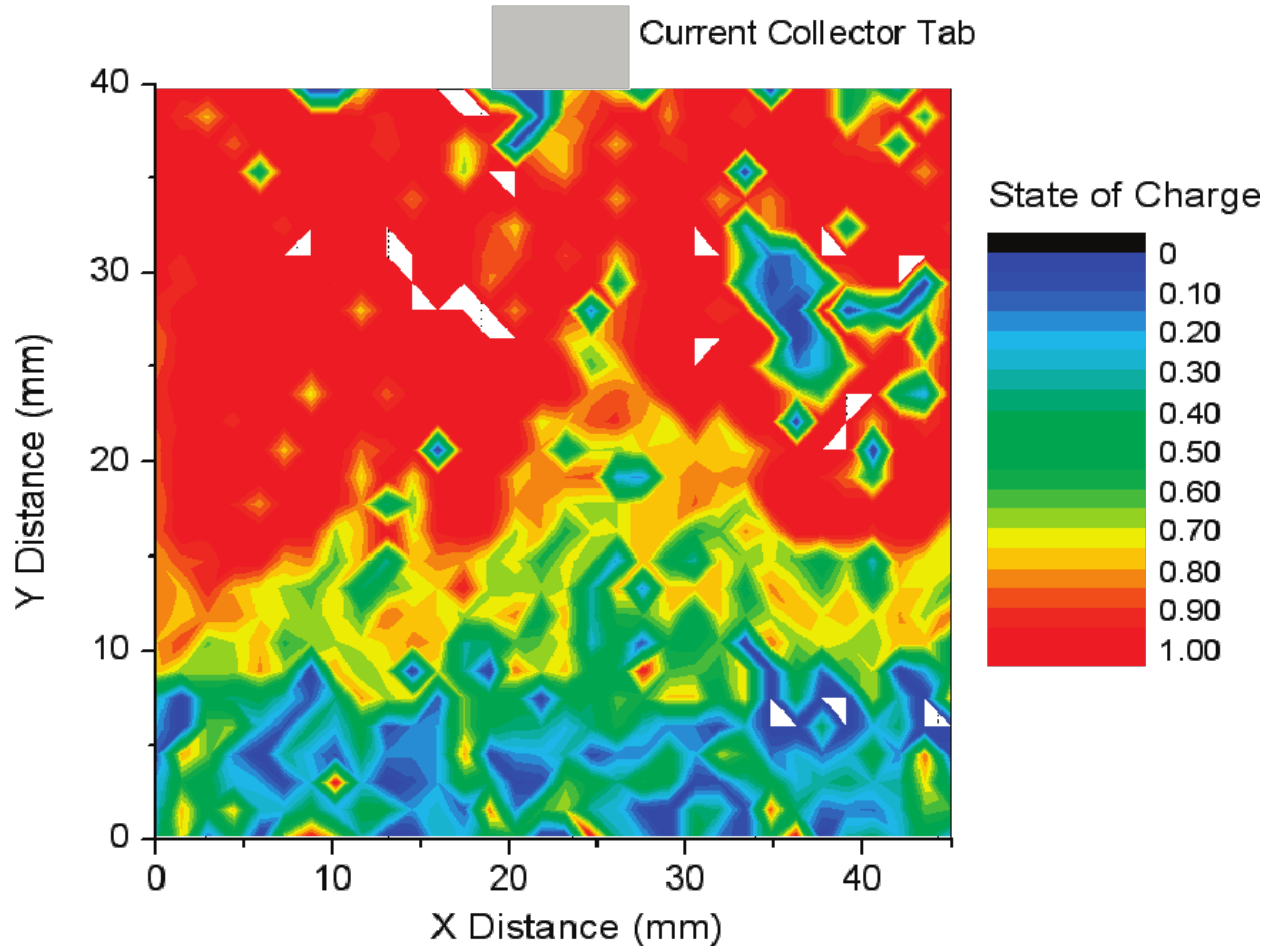


Figure 9:  $\text{FePO}_4$  phase concentration profile of the prismatic electrode at 50% state-of-charge.<sup>50</sup>

The penetrating power of high energy X-rays can make for a very compelling operando

experiment since the cell does not have to be modified, allowing conventional coin cells to be used. Strobridge et al. mapped the volume of a LiFePO<sub>4</sub> cathode in this way.<sup>36</sup> The incoming beam was scanned along the width and/or height of the cell and a collimator between the sample and detector allowed them to discriminate which gauge volume along the beam was being probed. The use of energy dispersive diffraction meant that the collimator did not limit the range of scattering vectors ( $q$ ) being sampled. This feature allowed for direct mapping of the entire volume. With this technique, they showed a clear relationship between electrode depth and state of charge, leading to valuable conclusions about the rate-limited steps in the reaction mechanism. They also uncovered inhomogeneities across the width of the electrode and used their measurements to validate a model exploring the effects of electrode porosity. A different approach does not limit the diffracted signal, but rather uses a tomographic setup to acquire diffraction projections and reconstruct the 3D volume. Jensen et al. analyzed coin-cell and 18650 cell batteries using tomography and high-energy diffraction.<sup>51</sup> Line scans were performed across the battery and at angles spanning 180° using a two-dimensional detector. The end result could be a full two-dimensional diffraction pattern at every position on the reconstructed slice. In practice, the authors first integrated each projection pattern azimuthally to a one-dimensional diffractogram and then performed a reconstruction for each scattering vector length,  $q$ . The two-dimensional diffraction pattern contains texture and strain information<sup>52</sup> that is lost when dimensionality is reduced. This feature was exploited by the authors by also separately integrating radially to map inhomogeneities in the preferred orientation of the LiCoO<sub>2</sub> cathode material. The 70 KeV radiation used passes easily through the case material, allowing the measurements to be performed *in situ* (though not *operando*), avoiding any effects caused by disassembly of the cell.

Combining tomography and XANES microscopy generates a very rich dataset that provides a window into the chemical environment at every point in the specimen. Meirer et al. used 3D XANES to probe the conversion of NiO to Ni metal in a discharged battery cathode.<sup>20</sup> By comparing the spectrum at each voxel (3D pixel) in a sample where the

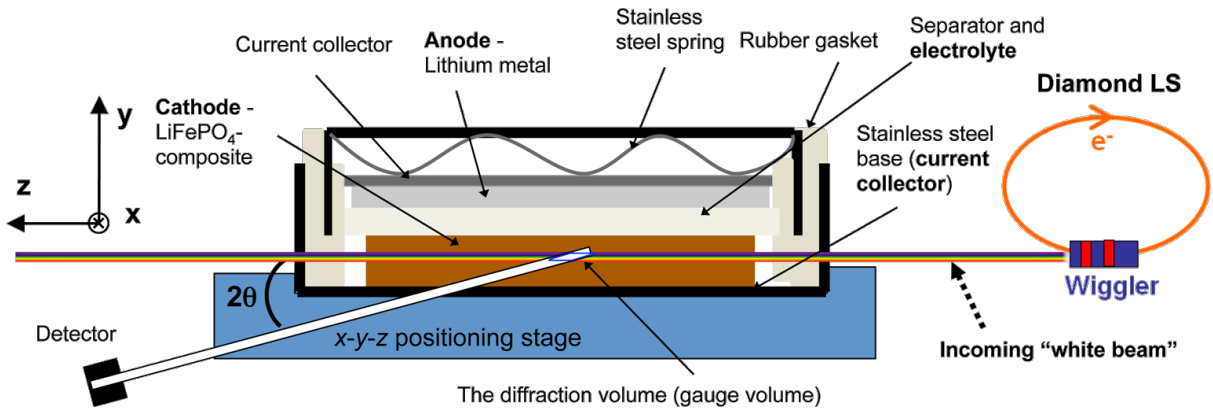


Figure 10: In situ EDXRD setup at the Diamond Light Source and the cross section of a coin-cell battery placed on an x-y-z position stage. X-rays penetrate the stainless steel casing and the diffracted X-rays are detected at a fixed angle.<sup>36</sup>

transformation was only 50% complete to known reference spectra, they assigned them to either NiO, Ni metal or a 50:50 mixture of the two. Additionally, they analyzed virtual slices through the three-dimensional particle to determine how the chemical states were distributed. They found significant inhomogeneities across the particle that depended on its size, as well as evidence of fracturing caused by volume expansion during the reaction. In this case, fracture was revealed as the enabler of the phase progression into the particle, which critically relies on microstructural formatting to reach completion.

Performing these types of measurements operando has the ability to provide insights that are not available with other techniques. The first demonstration of operando X-ray spectroscopy using a full-field technique involved the study of the reduction of CuO particles inside a coin-cell modified with Kapton windows.<sup>53</sup> A distinct shell of reduced copper metal was seen surrounded an unreacted CuO core, along with an intermediate Cu<sub>2</sub>O phase. A further iteration of this coin-cell design was developed by Yu et al. and used to study LiMn<sub>2</sub>O<sub>4</sub> spinel crystals. In order to improve resolution across the board, the emphasis in the design was placed on minimizing the thickness of absorbing materials, such as aluminum, and, for instance, it relied on 1 μm thick silicon nitride windows. The design was applied to the study of the transformation  $\text{Li}_2\text{Mn}_2\text{O}_4 \rightleftharpoons \text{LiMn}_2\text{O}_4 \rightleftharpoons \text{Mn}_2\text{O}_4$ .<sup>54</sup> During the experiment, the authors found significant local effects in the oxidation of the particles, wherein oxidized

(ii)

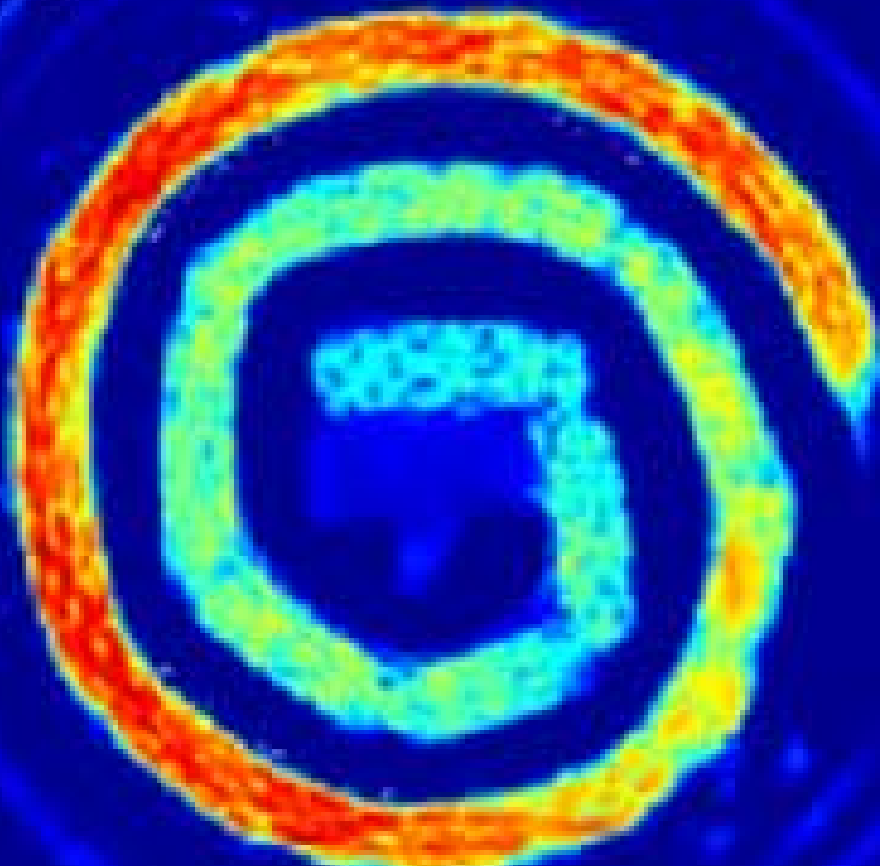


Figure 11: Data collected for cycled Ni-MH cell showing intensity at  $q = 1.36 \text{ \AA}^{-1}$ , representing the cathode phase.<sup>51</sup> Copyright The Authors 2015, Published by ECS. Creative Commons Attribution 4.0 License (CC-BY). Full text: <http://jes.ecsdl.org/content/162/7/A1310.full>

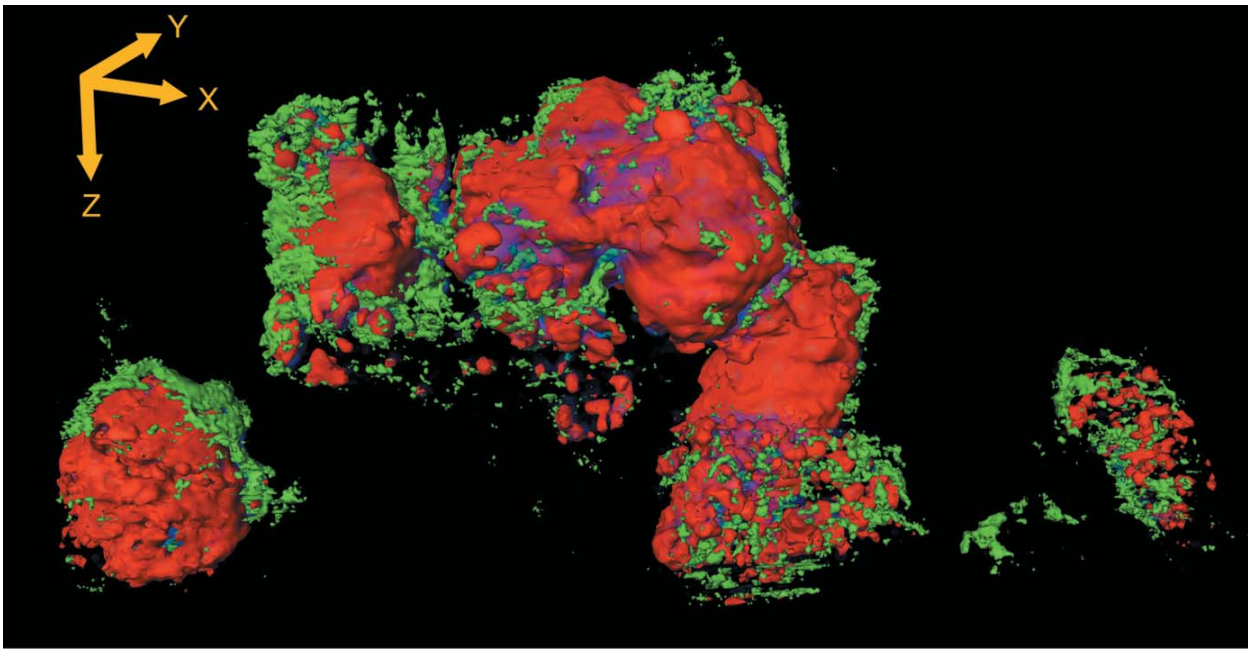


Figure 12: Reconstructed three-dimensional XANES tomography perspective rendering of three-dimensional data set of NiO cathode.<sup>20</sup> Reproduced with permission of the International Union of Crystallography.

$\text{LiMn}_2\text{O}_4$  regions formed and propagated through the crystal. Additionally, a reduced tetragonal  $\text{Li}_2\text{Mn}_2\text{O}_4$  phase persisted at potentials well above its predicted stability, according to the phase diagram, leading to a non-equilibrium coexistence with highly oxidized phases. These observations would probably not have been possible under ex situ conditions, where this situation would be expected to equilibrate. At higher potentials, several cracks in the crystals were seen that correlated with preferential oxidation to the fully delithiated  $\text{Mn}_2\text{O}_4$  phase, as seen in figure 13. The authors speculated that these cracks provide additional, fresh interfaces to facilitate phase transformation.<sup>55</sup>

Thanks to advances in the design of operando cells brought about by microfluidics, scanning TXM using soft X-rays has been recently demonstrated, and used to probe the spatial dynamics of  $\text{LiFePO}_4$  particles.<sup>40</sup> The authors were able to collect chemical images at a variety of rates while gathering reliable electrochemical data. Linear combination fitting was used to create maps of lithiated and delithiated material. It was found that the pathways upon lithiation and delithiation were strikingly different depending on the conditions of cy-

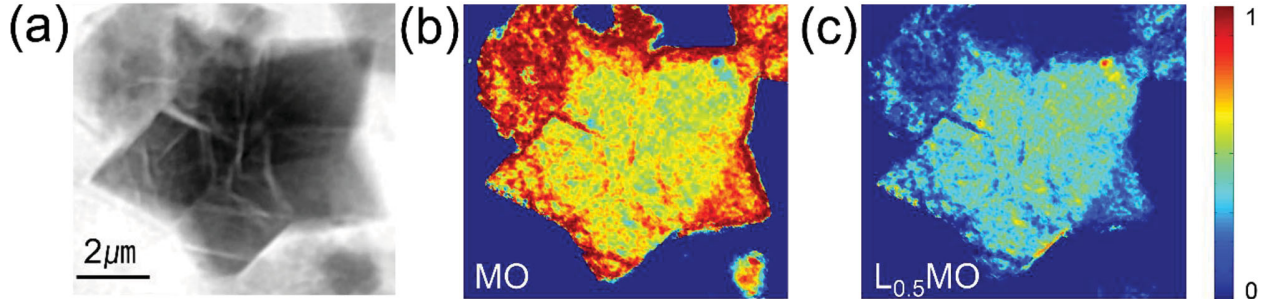


Figure 13: Preferential growth of Mn<sub>2</sub>O<sub>4</sub> along cracks at 4.09 V. (a) Inverted optical density image collected at 6700 eV. Heat maps where color contrast scales with the ratio of spectral standards of (b) Mn<sub>2</sub>O<sub>4</sub> and (c) Li<sub>0.5</sub>Mn<sub>2</sub>O<sub>4</sub> in each pixel. Reprinted with permission from Yu et al. Nonequilibrium Pathways during Electrochemical Phase Transformations in Single Crystals Revealed by Dynamic Chemical Imaging at Nanoscale Resolution. *Advanced Energy Materials* **2015**, 5. Copyright 2014 John Wiley and Sons.

pling. Thanks to the quality of the data, the authors were also able to extract the current density for actively (de)intercalating pixels. They found a strong dependence of the exchange current density ( $j_0$ ) and the degree of lithiation ( $x$  in  $\text{Li}_x\text{FePO}_4$ ), as shown in figure 14. Heterogeneities initially caused by other sources are then amplified by this positive feedback mechanism during lithiation and suppressed during delithiation.

Several other recent examples of operando TXM are worth highlighting. A study of LiFePO<sub>4</sub> provided details about the phase propagation mechanism and revealed inhomogeneities in the distribution of oxidized materials between multiple particles.<sup>56</sup> Li et al. studied FeF<sub>3</sub> and showed that the capacity loss seen in this material is due to incomplete conversion from Fe to Fe<sub>3</sub><sup>+</sup> during charging.<sup>25</sup> Another example further elucidates the role of oxygen species in lithium-air batteries. Olivares et al. looked at the formation of surface barriers, similar to the solid-electrolyte interface, on a carbon substrate. By examining the oxygen K-edge, they showed a relationship between particle morphology and the preference for forming carbonate, peroxide, and superoxide species.<sup>57</sup> The authors argued that the reactive and short-lived nature of some of these oxygen species ensures that meaningful results cannot be obtained without operando measurements.

Applications of operando Bragg diffraction microscopy are also available. Using a mi-

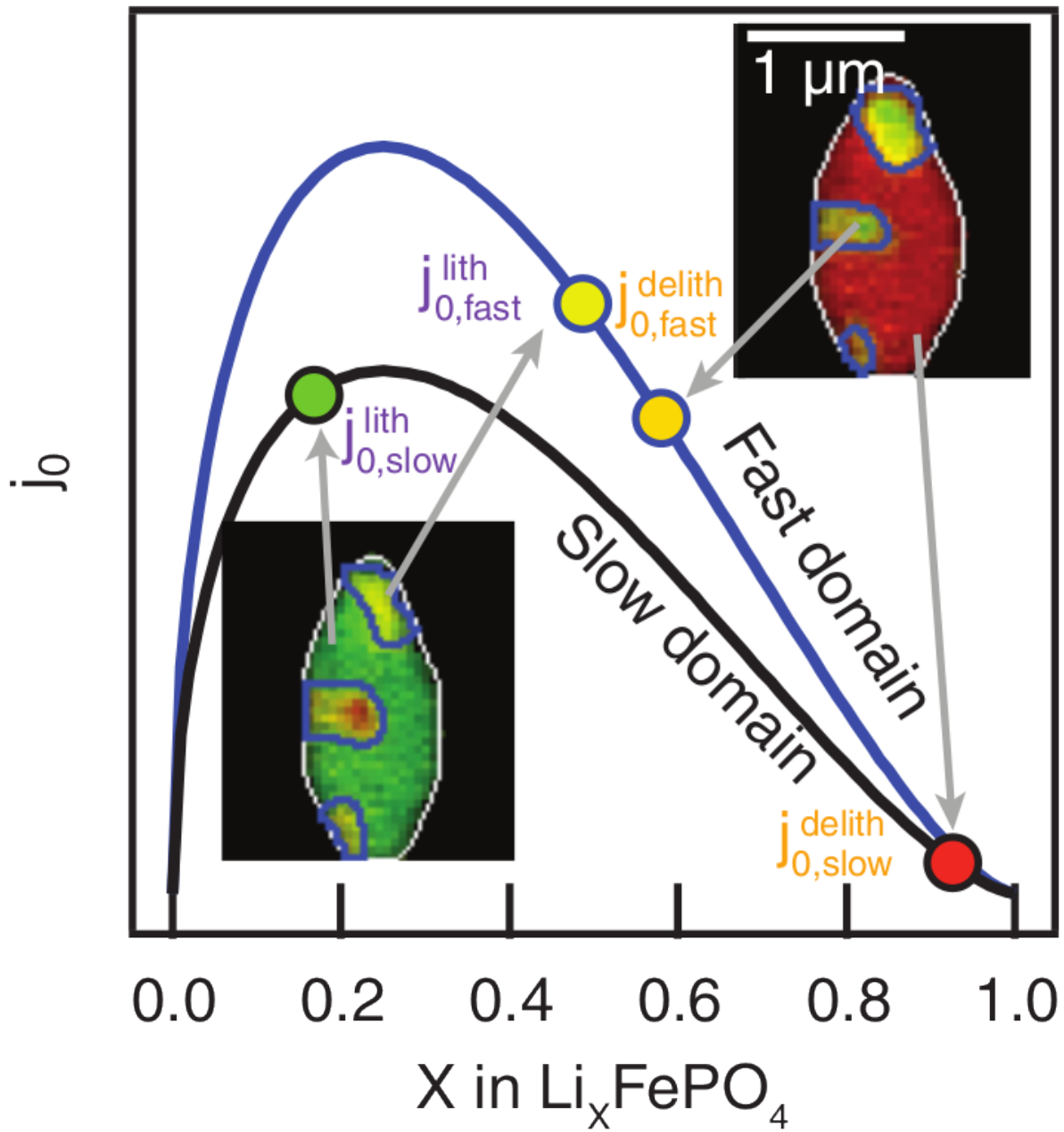


Figure 14: Relationship between measured exchange current density and degree of (de)lithiation. Because the skewed  $j_0$  peaks at  $x \approx 0.25$ , the value of  $j_0$  for the fast domains is several times that of  $j_0$  for the slow domains during delithiation, but the two quantities are comparable during lithiation. From Lim, J. et al. Origin and hysteresis of lithium compositional spatiodynamics within battery primary particles. *Science* **2016**, *353*, 566-571. Reprinted with permissions from AAAS.

croprobe of  $1.7\text{ }\mu\text{m}$ , Zhang et al. probed individual nanoscale LiFePO<sub>4</sub> crystallites.<sup>58</sup> Slight rotation of the sample illuminated several crystallites that satisfied the diffraction condition. Each crystallite was resolved because they were represented by a unique spot on the diffraction ring in the two-dimensional diffraction pattern. By following each of those spots through (dis)charge, the homogeneity and nature of the phase transformation was examined. They found that at a slower rate of (dis)charge the phase transformation occurs more homogeneously and gradually, while faster rates see the advent of defined phase boundaries.<sup>58</sup>

A similar strategy, relying on resolving crystallites through unique diffraction spots in the Debye ring was also applied to Bragg coherent diffraction, this time using LiNi<sub>0.5</sub>Mn<sub>1.5</sub>O<sub>4</sub> as the case study.<sup>59</sup> However, given its lensless character, the power of this contrast mode is exemplified by studies where phenomena within a particle were resolved through reconstructions of its three-dimensional volume using operando CDI. The specifics of the technique are also well suited to mapping strain within the particle. Ulvestad et al. released a series of papers using this technique. They first demonstrated its validity by mapping the strain and displacement of material within a particle.<sup>60</sup> The strain evolution of LiNi<sub>0.5</sub>Mn<sub>1.5</sub>O<sub>4</sub> was studied during charge/discharge and it was shown that significant gradients exist right before the phase transformation, shown in figure 15.<sup>61</sup> Lastly, they used strain maps to infer the existence of crystallographic defects within the crystallite and observed that these defects move as a function of charge-state.<sup>62</sup> They were able to characterize the dislocation by studying the displacement field around it. Additionally, they quantified strain anisotropy, leading to the proposal of a hinge-like structure between the unit-cell layers that moves more freely once sufficient lithium is removed. Based on similar observations made during discharge, it was shown that an initial lithium-rich phase expands throughout the particle, rather than multiple nucleation sites appearing; this result suggests that within a single particle, the reaction pathway was close to thermodynamic equilibrium in the conditions employed.

Interpretation of two dimensional imaging data is often confounded by the fact that the measured intensity at each position is a projection through the entire specimen. Tomography

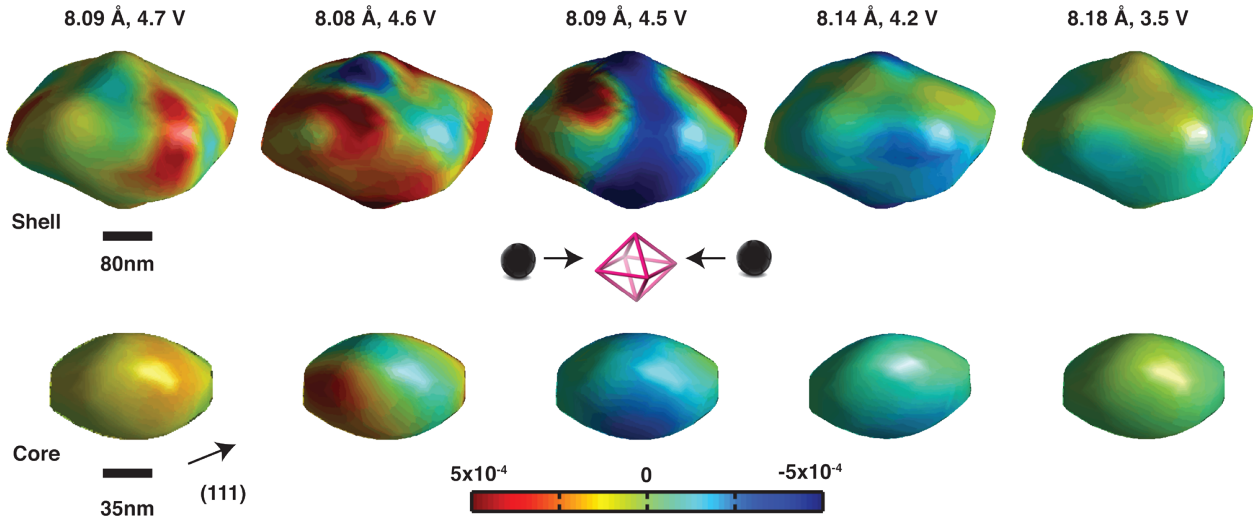


Figure 15: Isosurface projections of strain evolution in  $\text{LiNi}_{0.5}\text{Mn}_{1.5}\text{O}_4$  nanoparticle. The shell and core both show inhomogeneous strain during discharge. Images are labeled by their respective lattice constant values and open circuit voltages. The highest lattice strain occurs immediately prior to the phase transformation.<sup>61</sup>

neatly solves this problem, and operando tomography will be a key technique in fully understanding battery material mechanisms. Despite the very long acquisition times required, some recent publications show the power of this technique. In conversion reactions, mixtures of relatively heavy metallic particles and  $\text{Li}_2\text{O}$  are formed.<sup>63</sup> Since the differences in attenuation coefficients of the different species is quite large, quantification of changes in contrast in the image can be used to create pseudo-chemical maps. This approach is relatively fast since data only needs to be collected over one X-ray energy. This idea was first exploited by Ebner et al. to study the reduction of tin oxide. A core-shell mechanism was observed as well as detailed information about crack initiation and growth. They also compared particle-level volume changes and their relationship to the expansion of the electrode as a whole. They found that the particles expand beyond the tolerance of the supporting matrix, which has implications for the reversibility of the cell.<sup>64</sup> A similar approach to the analysis of individual tin oxide particles during the first two charge-discharge cycles showed significant fracturing and pulverization, with an accompanying loss in reversible capacity.<sup>65</sup> This approach is only valid for three-dimensional imaging since in two-dimensions the intensity of a given pixel

is heavily influenced by the thickness of the sample at that point. The majority of reactions of interest in batteries involve compounds that do not show significant differences in attenuation coefficient. In this case, X-ray absorbance tomography is needed. The only available example highlights the challenge of interpreting projection images directly. Wang et al. collected a 46-point spectrum across the iron K-edge of a LiFePO<sub>4</sub> cathode particle and developed a run-out correction system to enable automated tomography. In order to accommodate the significant overhead in time required to acquire 2D images at different energy and angle, the battery was charged extremely slowly (10-100 times slower than would be realistic). Nonetheless, the insight collected was noteworthy, with the advent of a clear core-shell structure, as shown in figure 16. When considering two-dimensional projections from only one angle, it appears as though a mixed state existed between the lithiated and delithiated states. Tomographic reconstruction reveals that this mixed state is not present anywhere in the particle and is merely an artifact of the projection process.<sup>27</sup>

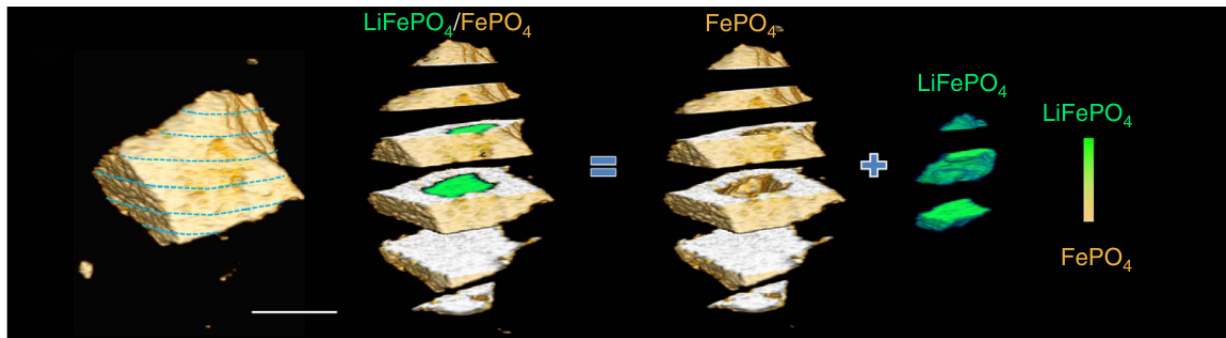


Figure 16: Sliced view of LiFePO<sub>4</sub> at highly delithiated state. The sliced view reveals 3D internal core-shell phase distribution. Scale bar, 10 μm. Reprinted from reference,<sup>27</sup> licensed under CC-BY 4.0.

## Future Outlook

The impact that X-ray imaging and mapping have already had in our understanding of electrochemical reactions relevant to batteries is significant. This perspective demonstrates that it is currently possible to resolve chemical phenomena at the level of individual par-

ticles, at resolutions as low as 10 nm, and, in some case, while the material is subject to working conditions. However, the wealth of techniques presented here and the incipience of these approaches lead to the conclusion that researchers are only beginning to exploit the information that can be collected. We have emphasized the importance of appropriately defining the goals of the experiment in terms of chemical, spatial and temporal resolution. The three cannot currently be attained at the same time in an experiment that is directly relevant to function, with compromises leading to loss of chemical information in most cases. It is also important to recognize and understand the interaction between the beam and the material, especially when molecules sensitive to radiation, such as the organic solvents in a battery electrolyte, are present. This understanding is currently extremely rudimentary, so systematic studies should be incentivized.

When it comes to operando measurements, further improvements in measurement protocols and cell design are necessary. Data analysis “on the fly” would provide valuable input to the experimenter in terms of defining the chances of success of the experiment and creating options for data minimization and experiment optimization. When it comes to experimental environments, the higher the resolution desired, the heavier the need for engineering cells that notably differ from conventional battery setups such as coin or even prismatic cells. This design often imposes conditions that are not representative, or where quantitative electroanalysis simultaneous to the observations is not possible, inducing a critical loss of information. Further, given the ultimate goal of guiding improvements in battery performance, it is important that the design of operando cells takes into account the importance of preserving the fidelity of the electrochemical responses to those that define function in a device.

As the community increases its awareness of the unique capabilities of X-ray microscopes, it is expected that their use in battery research will continue to grow. Since chemical imaging is only possible at a synchrotron, this growth will contribute to a vibrant and diverse user community. The fact that synchrotron scientists continue to improve existing setups and

design new modes of imaging will contribute to the presence of X-ray chemical imaging and mapping in battery research. In this context, the availability of access to the synchrotron facilities where the measurements are performed is likely to become an even more pronounced limiting factor to be tackled by the agencies managing the facilities. A solution would involve improvements in the flux and brightness of the X-ray source to decrease measurement times. Indeed, many facilities are in the process of upgrading their storage rings to provide X-rays to enable techniques with increased complexity, while shortening the measurement times for those that are already possible today. The National Synchrotron Light Source II (NSLS-II) has now replaced the original NSLS at Brookhaven. Additionally, the Advanced Photon Source (APS), Advanced Light Source, Stanford Synchrotron Radiation Lightsource, and Cornell High Energy Synchrotron Source (United States), as well Deutsches Elektronen-Synchrotron and European Synchrotron Radiation Facility in Europe, and Spring-8 in Japan all have plans for upgrading in the future, though many of these are still in very early planning stages. These improvements promise brighter and more coherent X-rays. The APS-U project also promises X-ray beams that will be much smaller in the horizontal direction, allowing more of the beam to be focused on the sample for imaging applications. The coherence of the X-rays is critical for ptychography and CDI; having pervasive access to coherent radiation will make these imaging techniques faster and more efficient than today. Increased brightness will shorten the time needed to acquire a dataset of sufficient quality for analysis. These developments would bring experiments without compromises in any of the dimensions of resolution closer to reality. In other words, it would translate into an increase in the time resolution of operando experiments without sacrificing spatial or chemical resolution and will facilitate the next generation of high-impact experiments. Both operando and three-dimensional analyses have demonstrated their ability to generate insights that would otherwise go unnoticed: combining them in a robust and practical way will likely be at the forefront of battery imaging techniques. These developments will surely drastically improve the way that we are able to define relevant reactions, at the level of molecules to architectures,

providing vital inputs for the design of devices that break current barriers of performance.

## Acknowledgement

This work was supported as part of the NorthEast Center for Chemical Energy Storage (NECCES), an Energy Frontier Research Center funded by the U.S. Department of Energy, Office of Science, Basic Energy Sciences under Award # DE-SC0012583.

## References

- (1) Whittingham, M. S. History, Evolution, and Future Status of Energy Storage. *Proceedings of the IEEE* **2012**, *100*, 1518–1534.
- (2) M. Armand, J. T. Building Better Batteries. *Nature* **2008**,
- (3) Newman, J. Optimization of Porosity and Thickness of a Battery Electrode by Means of a Reaction-Zone Model. *Journal of The Electrochemical Society* **1995**, *142*, 97–101.
- (4) Wu, S.-L.; Javier, A. E.; Devaux, D.; Balsara, N. P.; Srinivasan, V. Discharge Characteristics of Lithium Battery Electrodes with a Semiconducting Polymer Studied by Continuum Modeling and Experiment. *Journal of The Electrochemical Society* **2014**, *161*, A1836–A1843.
- (5) Palacin, M. R. Recent Advances in Rechargeable Battery Materials: A Chemist’s Perspective. *Chem. Soc. Rev.* **2009**, *38*, 2565–2575.
- (6) Holt, M.; Harder, R.; Winarski, R.; Rose, V. Nanoscale Hard X-Ray Microscopy Methods for Materials Studies. *Annual Review of Materials Research* **2013**, *43*, 183–211.
- (7) Maire, E.; Withers, P. J. Quantitative X-ray tomography. *International Materials Reviews* **2014**, *59*, 1–43.

- (8) Chae, S. R.; Moon, J.; Yoon, S.; Bae, S.; Levitz, P.; Winarski, R.; Monteiro, P. J. M. Advanced Nanoscale Characterization of Cement Based Materials Using X-Ray Synchrotron Radiation: A Review. *International Journal of Concrete Structures and Materials* **2013**, *7*, 95–110.
- (9) Tsuji, K.; Matsuno, T.; Takimoto, Y.; Yamanashi, M.; Kometani, N.; Sasaki, Y. C.; Hasegawa, T.; Kato, S.; Yamada, T.; Shoji, T.; Kawahara, N. New Developments of X-ray Fluorescence Imaging Techniques in Laboratory. *Spectrochimica Acta Part B: Atomic Spectroscopy* **2015**, *113*, 43 – 53.
- (10) Shapiro, D. A.; Yu, Y.-S.; Tyliszczak, T.; Cabana, J.; Celestre, R.; Chao, W.; Kaznatcheev, K.; Kilcoyne, D. A. L.; Maia, F.; Marchesini, S.; Meng, Y. S.; Warwick, T.; Yang, L. L.; Padmore, H. A. Chemical Composition Mapping with Nanometre Resolution by Soft X-ray Microscopy. *Nature Photonics* **2014**, *8*, 765–769.
- (11) Guinebretière, R. *X-ray Diffraction by Polycrystalline Materials*; ISTE Ltd, 2007; pp 39–48.
- (12) Mobilio, S.; Boscherini, F.; Meneghini, C. *Synchrotron Radiation*; Springer-Verlag Berlin Heidelberg, 2015.
- (13) SESAME holds its second user's meeting. *Journal of Synchrotron Radiation* **2004**, *11*, 214–215.
- (14) Ice, G. E.; Pang, J. W. Tutorial on x-ray microLaue diffraction. *Materials Characterization* **2009**, *60*, 1191–1201.
- (15) Pelt, D. M.; Batenburg, K. J. Fast Tomographic Reconstruction From Limited Data Using Artificial Neural Networks. *IEEE Transactions on Image Processing* **2013**, *22*, 5238–5251.

- (16) Snigirev, A.; Kohn, V.; Snigireva, I.; Lengeler, B. A compound refractive lens for focusing high-energy X-rays. *Nature* **1996**, *384*, 49–51.
- (17) Kirkpatrick, P.; Baez, A. V. Formation of Optical Images by X-Rays. *J. Opt. Soc. Am.* **1948**, *38*, 766–774.
- (18) Fresnel Zone Plate Theory. <http://zoneplate.lbl.gov/theory>, Accessed: 2016-11-04.
- (19) Yan, H.; Conley, R.; Bouet, N.; Chu, Y. S. Hard x-ray nanofocusing by multilayer Laue lenses. *Journal of Physics D: Applied Physics* **2014**, *47*, 263001.
- (20) Meirer, F.; Cabana, J.; Liu, Y.; Mehta, A.; Andrews, J.; Pianetta, P. Three-dimensional Imaging of Chemical Phase Transformations at the Nanoscale with Full-Field Transmission X-ray Microscopy. *Journal of Synchrotron Radiation* **2011**, *18*, 773–781.
- (21) Li, Y.; Weker, J. N.; Gent, W. E.; Mueller, D. N.; Lim, J.; Cogswell, D. A.; Tyliszczak, T.; Chueh, W. C. Dichotomy in the Lithiation Pathway of Ellipsoidal and Platelet LiFePO<sub>4</sub> Particles Revealed through Nanoscale Operando State-of-Charge Imaging. *Advanced Functional Materials* **2015**, *25*, 3677–3687.
- (22) Kim, J. W.; Manna, S.; Dietze, S. H.; Ulvestad, A.; Harder, R.; Fohtung, E.; Fullerton, E. E.; Shpyrko, O. G. Curvature-induced and thermal strain in polyhedral gold nanocrystals. *Applied Physics Letters* **2014**, *105*.
- (23) Harmon, K. J.; Bennett, E. E.; Gomella, A. A.; Wen, H. Efficient Decoding of 2D Structured Illumination with Linear Phase Stepping in X-Ray Phase Contrast and Dark-Field Imaging. *PLOS ONE* **2014**, *9*, 1–6.
- (24) Takahashi, Y.; Suzuki, A.; Zettsu, N.; Kohmura, Y.; Yamauchi, K.; Ishikawa, T. Multiscale Element Mapping of Buried Structures by Ptychographic X-ray Diffraction Microscopy Using Anomalous Scattering. *Applied Physics Letters* **2011**, *99*.

- (25) Li, L.; Chen-Wiegart, Y.-c. K.; Wang, J.; Gao, P.; Ding, Q.; Yu, Y.-S.; Wang, F.; Cabana, J.; Wang, J.; Jin, S. Visualization of Electrochemically Driven Solid-State Phase Transformations Using Operando Hard X-ray Spectro-imaging. *Nat Commun* **2015**, *6*.
- (26) Yin, G.-C.; Tang, M.-T.; Song, Y.-F.; Chen, F.-R.; Liang, K. S.; Duewer, F. W.; Yun, W.; Ko, C.-H.; Shieh, H.-P. D. Energy-tunable Transmission X-ray Microscope for Differential Contrast Imaging with Near 60 nm Resolution Tomography. *Applied Physics Letters* **2006**, *88*.
- (27) Wang, J.; Karen Chen-Wiegart, Y.-C.; Eng, C.; Shen, Q.; Wang, J. Visualization of Anisotropic-Isotropic Phase Transformation Dynamics in Battery Electrode Particles. *Nature Communications* **2016**, *7*, 12372.
- (28) Yu, Y.-S. et al. Dependence on Crystal Size of the Nanoscale Chemical Phase Distribution and Fracture in  $\text{Li}_x\text{FePO}_4$ . *Nano Letters* **2015**, *15*, 4282–4288.
- (29) Shlens, J. A Tutorial on Independent Component Analysis. **2014**,
- (30) Knuth, K. H. Informed Source Separation: A Bayesian Tutorial. *Proceedings of the 13th European Signal Processing Conference* **2005**,
- (31) Bioucas-Dias, J. M.; Plaza, A. An overview on hyperspectral unmixing: Geometrical, statistical, and sparse regression based approaches. *Geoscience and Remote Sensing Symposium (IGARSS)*, 2011 IEEE International. 2011; pp 1135–1138.
- (32) Duarte, L. T.; Moussaoui, S.; Jutten, C. Source Separation in Chemical Analysis : Recent achievements and perspectives. *IEEE Signal Processing Magazine* **2014**, *31*, 135–146.
- (33) Boesenborg, U.; Meirer, F.; Liu, Y.; Shukla, A.; Dell'Anna, R.; Tyliszczak, T.; Chen, G.; Andrews, J.; Richardson, T.; Kostecki, R.; Cabana, J. Mesoscale Phase Distribution in

Single Particles of LiFePO<sub>4</sub> following Lithium Deintercalation. *Chemistry of Materials* **2013**, *25*, 1664–1672.

- (34) Deb, A.; Cairns, E. J. In situ X-ray absorption spectroscopy-A probe of cathode materials for Li-ion cells. *Fluid Phase Equilibria* **2006**, *241*, 4 – 19.
- (35) Kämpfe, B.; Luczak, F.; Michel, B. Energy Dispersive X-Ray Diffraction. *Particle & Particle Systems Characterization* **2005**, *22*, 391–396.
- (36) Strobridge, F. C.; Orvananos, B.; Croft, M.; Yu, H.-C.; Robert, R.; Liu, H.; Zhong, Z.; Connolley, T.; Drakopoulos, M.; Thornton, K.; Grey, C. P. Mapping the Inhomogeneous Electrochemical Reaction Through Porous LiFePO<sub>4</sub>-Electrodes in a Standard Coin Cell Battery. *Chemistry of Materials* **2015**, *27*, 2374–2386.
- (37) Robinson, I.; Harder, R. Coherent X-ray diffraction imaging of strain at the nanoscale. *Nat Mater* **2009**, *8*, 291–298.
- (38) Venkatakrishnan, S. V.; Farmand, M.; Yu, Y. S.; Majidi, H.; van Benthem, K.; Marchesini, S.; Shapiro, D. A.; Hexemer, A. Robust X-Ray Phase Ptycho-Tomography. *IEEE Signal Processing Letters* **2016**, *23*, 944–948.
- (39) Liu, H.; Strobridge, F. C.; Borkiewicz, O. J.; Wiaderek, K. M.; Chapman, K. W.; Chupas, P. J.; Grey, C. P. Capturing metastable structures during high-rate cycling of LiFePO<sub>4</sub> nanoparticle electrodes. *Science* **2014**, *344*.
- (40) Lim, J.; Li, Y.; Alsem, D. H.; So, H.; Lee, S. C.; Bai, P.; Cogswell, D. A.; Liu, X.; Jin, N.; Yu, Y.-s.; Salmon, N. J.; Shapiro, D. A.; Bazant, M. Z.; Tyliszczak, T.; Chueh, W. C. Origin and hysteresis of lithium compositional spatiodynamics within battery primary particles. *Science* **2016**, *353*, 566–571.
- (41) Borkiewicz, O. J.; Wiaderek, K. M.; Chupas, P. J.; Chapman, K. W. Best Practices for Operando Battery Experiments: Influences of X-ray Experiment Design on Observed

Electrochemical Reactivity. *The Journal of Physical Chemistry Letters* **2015**, *6*, 2081–2085.

- (42) Lin, C.-K.; Ren, Y.; Amine, K.; Qin, Y.; Chen, Z. In situ high-energy X-ray diffraction to study overcharge abuse of 18650-size lithium-ion battery. *Journal of Power Sources* **2013**, *230*, 32 – 37.
- (43) Borkiewicz, O. J.; Shyam, B.; Wiaderek, K. M.; Kurtz, C.; Chupas, P. J.; Chapman, K. W. The AMPIX Electrochemical Cell: a Versatile Apparatus for In Situ X-ray Scattering and Spectroscopic Measurements. *Journal of Applied Crystallography* **2012**, *45*, 1261–1269.
- (44) Whittingham, M. S. Ultimate Limits to Intercalation Reactions for Lithium Batteries. *Chemical Reviews* **2014**, *0*, null.
- (45) Balogun, M.-S.; Qiu, W.; Luo, Y.; Meng, H.; Mai, W.; Onasanya, A.; Olaniyi, T. K.; Tong, Y. A review of the development of full cell lithium-ion batteries: The impact of nanostructured anode materials. *Nano Research* **2016**, *9*, 2823–2851.
- (46) Eastwood, D.; Bradley, R.; Tariq, F.; Cooper, S.; Taiwo, O.; Gelb, J.; Merkle, A.; Brett, D.; Brandon, N.; Withers, P.; Lee, P.; Shearing, P. The application of phase contrast X-ray techniques for imaging Li-ion battery electrodes. *Nuclear Instruments and Methods in Physics Research Section B: Beam Interactions with Materials and Atoms* **2014**, *324*, 118 – 123.
- (47) Cooper, S.; Eastwood, D.; Gelb, J.; Damblanc, G.; Brett, D.; Bradley, R.; Withers, P.; Lee, P.; Marquis, A.; Brandon, N.; Shearing, P. Image based modelling of microstructural heterogeneity in LiFePO<sub>4</sub> electrodes for Li-ion batteries. *Journal of Power Sources* **2014**, *247*, 1033 – 1039.
- (48) Yang, F.; Liu, Y.; Martha, S. K.; Wu, Z.; Andrews, J. C.; Ice, G. E.; Pianetta, P.; Nanda, J. Nanoscale Morphological and Chemical Changes of High Voltage Lithium-

Manganese Rich NMC Composite Cathodes with Cycling. *Nano Letters* **2014**, *14*, 4334–4341.

- (49) Lin, F.; Nordlund, D.; Li, Y.; Quan, M. K.; Cheng, L.; Weng, T.-C.; Liu, Y.; Xin, H. L.; Doeff, M. M. Metal segregation in hierarchically structured cathode materials for high-energy lithium batteries. *Nature Energy* **2016**, *1*, 15004 EP –.
- (50) Liu, J.; Kunz, M.; Chen, K.; Tamura, N.; Richardson, T. Visualization of Charge Distribution in a Lithium Battery Electrode. *The Journal of Physical Chemistry Letters* **2010**, *1*, 2120–2123.
- (51) Jensen, K. M. Ø.; Yang, X.; Laveda, J. V.; Zeier, W. G.; See, K. A.; Michiel, M. D.; Melot, B. C.; Corr, S. A.; Billinge, S. J. L. X-Ray Diffraction Computed Tomography for Structural Analysis of Electrode Materials in Batteries. *Journal of The Electrochemical Society* **2015**, *162*, A1310–A1314.
- (52) *Two-Dimensional X-Ray Diffraction*; John Wiley & Sons, Inc., 2009; pp 219,249.
- (53) Wang, J.; Chen-Wiegart, Y.-c. K.; Wang, J. In situ chemical mapping of a lithium-ion battery using full-field hard X-ray spectroscopic imaging. *Chem. Commun.* **2013**, *49*, 6480–6482.
- (54) Ohzuku, T.; Kitagawa, M.; Hirai, T. Electrochemistry of Manganese Dioxide in Lithium Nonaqueous Cell. *Journal of The Electrochemical Society* **1990**, *137*, 769–775.
- (55) Yu, Y.-S.; Kim, C.; Liu, Y.; van der Ven, A.; Meng, Y. S.; Kostecki, R.; Cabana, J. Nonequilibrium Pathways during Electrochemical Phase Transformations in Single Crystals Revealed by Dynamic Chemical Imaging at Nanoscale Resolution. *Advanced Energy Materials* **2015**, *5*.
- (56) Wang, J.; Chen-Wiegart,; Karen, Y.-c.; Wang, J. In operando tracking phase transfor-

- mation evolution of lithium iron phosphate with hard X-ray microscopy. *Nat Commun* **5**.
- (57) Olivares-Marín, M.; Sorrentino, A.; Lee, R.-C.; Pereiro, E.; Wu, N.-L.; Tonti, D. Spatial Distributions of Discharged Products of Lithium-Oxygen Batteries Revealed by Synchrotron X-ray Transmission Microscopy. *Nano Letters* **2015**, *15*, 6932–6938.
- (58) Zhang, X.; van Hulzen, M.; Singh, D. P.; Brownrigg, A.; Wright, J. P.; van Dijk, N. H.; Wagemaker, M. Direct view on the phase evolution in individual LiFePO<sub>4</sub> nanoparticles during Li-ion battery cycling. *Nature Communications* **2015**, *6*.
- (59) Singer, A.; Ulvestad, A.; Cho, H.-M.; Kim, J. W.; Maser, J.; Harder, R.; Meng, Y. S.; Shpyrko, O. G. Nonequilibrium Structural Dynamics of Nanoparticles in LiNi<sub>1/2</sub>Mn<sub>3/2</sub>O<sub>4</sub> Cathode under Operando Conditions. *Nano Letters* **2014**, *14*, 5295–5300.
- (60) Ulvestad, A.; Cho, H. M.; Harder, R.; Kim, J. W.; Dietze, S. H.; Fohtung, E.; Meng, Y. S.; Shpyrko, O. G. Nanoscale strain mapping in battery nanostructures. *Applied Physics Letters* **2014**, *104*.
- (61) Ulvestad, A.; Singer, A.; Cho, H.-M.; Clark, J. N.; Harder, R.; Maser, J.; Meng, Y. S.; Shpyrko, O. G. Single Particle Nanomechanics in Operando Batteries via Lensless Strain Mapping. *Nano Letters* **2014**, *14*, 5123–5127.
- (62) Ulvestad, A.; Singer, A.; Clark, J. N.; Cho, H. M.; Kim, J. W.; Harder, R.; Maser, J.; Meng, Y. S.; Shpyrko, O. G. Topological defect dynamics in operando battery nanoparticles. *Science* **2015**, *348*, 1344–1347.
- (63) Cabana, J.; Monconduit, L.; Larcher, D.; Palacín, M. R. Beyond Intercalation-Based Li-Ion Batteries: The State of the Art and Challenges of Electrode Materials Reacting Through Conversion Reactions. *Advanced Materials* **2010**, *22*, E170–E192.

- (64) Ebner, M.; Marone, F.; Stampanoni, M.; Wood, V. Visualization and Quantification of Electrochemical and Mechanical Degradation in Li Ion Batteries. *Science* **2013**, *342*, 716–720.
- (65) Wang, J.; Chen-Wiegart, Y.-c. K.; Wang, J. In Situ Three-Dimensional Synchrotron X-Ray Nanotomography of the (De)lithiation Processes in Tin Anodes. *Angewandte Chemie International Edition* **2014**, *53*, 4460–4464.

## Biographies

### Mark Wolf

Mark Wolf is a Ph.D. candidate at the University of Illinois Chicago performing research on cathode materials using ptychography and operando X-ray microscopy. He received a Bachelor of Science from Western Michigan University in 2008 with a dual-major in chemistry and music.

### Brian M. May

Brian May is a Ph.D. candidate at the University of Illinois at Chicago in Dr. Jordi Cabana's group. Prior to his time at UIC, he received his B.S. in chemistry from Loyola University Chicago in 2013, and researched allosteric activation mechanisms and protein crystal structures with Dr. Miguel Ballicora and Dr. Dali Liu. His current research focuses on developing new synchrotron techniques for applications in understanding the chemical reactions of battery cathode materials.

### Jordi Cabana

Jordi Cabana is an Assistant Professor at the Department of Chemistry of the University of Illinois at Chicago. Prior to his appointment at UIC, he was a Research Scientist at Lawrence

Berkeley National Laboratory (USA), from 2008 until 2013. Prof. Cabana completed his Ph.D. in Materials Science at the Institut de Ciència de Materials de Barcelona (Spain) in 2004, and worked in the Department of Chemistry at Stony Brook University (USA) as a postdoctoral associate. He is generally interested in the physical and inorganic chemistry of materials, with emphasis on their redox and transport properties, and a focus on applications in electrochemical energy storage. Members of his group are frequent users of synchrotron techniques such as diffraction, spectroscopy and microscopy.

## Graphical TOC Entry

